EFFECTS OF TILTED AND FAULTED STRATA ON SEISMIC GROUND MOTION

Prepared for

U.S. Nuclear Regulatory Commission
Contract NRC–02–07–006

Prepared by

Amitava Ghosh
Simon Hsiung

Center for Nuclear Waste Regulatory Analyses
San Antonio, Texas

September 2011

ABSTRACT

This report documents the results of estimating seismic motion at the ground surface from an earthquake. The earthquake motion amplifies while traveling upward through the geologic medium. This amplification is dependent on the properties of the geologic medium. Reliable estimation of the ground motion is necessary for designing surface structures. Although traditionally a one-dimensional analysis is conducted to estimate the ground motion, in this study two-dimensional analyses are conducted to estimate the ground motion from an earthquake. The primary objective of this study is to assess the potential spatial variation of ground response from seismic waves in fractured and/or layered deposits, especially with a thick soil cover having varying thickness and extent. The purpose of the study is to develop an understanding of seismic response in a complex medium with varying soil thickness and extent. The UDEC™ code is used to simulate a fractured medium without material degradation, and the FLAC code is used to simulate a layered medium with material degradation. Results using UDEC show that the amplification of seismic motion is small, generally limited to approximately 1.5 times the input motion. However, with material degradation incorporated in the simulation using FLAC, the amplification could be large—several times the input motion. In addition, the estimated ground motion at the surface shows resonant behavior with long duration oscillations. These phenomena have been observed in different earthquake records, especially over thick soil deposits similar to those used in this study. The results are preliminary and require further investigation.

CONTENTS

FIGURES

FIGURES (continued)

Figure Page

TABLES

ACKNOWLEDGMENTS

This report was prepared to document work performed by the Center for Nuclear Waste Regulatory Analyses (CNWRA®) for the U.S. Nuclear Regulatory Commission (NRC) under Contract No. NRC–02–07–006. The activities reported here were performed on behalf of the NRC Office of Nuclear Material Safety and Safeguards, Division of High-Level Waste Repository Safety. The report is an independent product of CNWRA and does not necessarily reflect the views or regulatory position of NRC.
The authors gratefully acknowledge B. Dasgupta for his technical review, B. Sagar for his programmatic review, L. Mulverhill for her editorial review, and A. Ramos for his secretarial support.

QUALITY OF DATA, ANALYSES, AND CODE DEVELOPMENT

DATA: All CNWRA-generated data contained in this report meet quality assurance requirements described in the Geosciences and Engineering Division Quality Assurance Manual. Sources of other data should be consulted for determining the level of quality of those data.

ANALYSES AND CODES: UDEC Version 5.0 and FLAC Version 5.0 (Itasca Consulting Group, Inc., 2011; 2005) have been used in the analyses presented in this report. These codes are controlled under the CNWRA quality assurance program. Analyses described in this report are documented in CNWRA Scientific Notebook 889 (Ghosh, 2007).

REFERENCES

Ghosh, A. "Characterization of Effects of Faulted and Inclined Strata on Ground Response at the Proposed Site for Surface Facilities at the Potential Repository at Yucca Mountain." Scientific Notebook 889. San Antonio, Texas: Center for Nuclear Waste Regulatory Analyses. 33 p. 2007.

Itasca Consulting Group, Inc. "UDEC Version 5.0 User's Guide." Minneapolis, Minnesota: Itasca Consulting Group, Inc. 2011.

_____. "FLAC Fast Lagrangian Analysis of Continua User's Guide (Version 5.0)." Minneapolis, Minnesota: Itasca Consulting Group, Inc. 2005.

1 INTRODUCTION

1.1 Background and Purpose

An estimate of the seismic ground motion at the surface of the Earth is necessary to (i) develop design response spectra, (ii) evaluate dynamic stresses and strains for assessing liquefaction potential, and (iii) determine earthquake-induced force for assessing stability of Earth-retaining structures (Kramer, 1996). Generally, empirical ground motion relationships (attenuation relationships), based on characteristics of previously recorded earthquakes, are used to estimate the seismic motion at the bedrock of a given site. The ground response analysis is used to assess the response of the soil or rock medium subjected to the seismic motion at the bedrock.

Over the years, a number of different techniques have been developed to estimate the surface motion from an earthquake. Both linear and nonlinear models have been used to approximate the material behavior when subjected to an earthquake motion. Analyses also have been conducted in one, two, and three dimensions. The Center for Nuclear Waste Regulatory Analyses (CNWRA®) conducted analyses to simulate the ground response using a one-dimensional (1D) model with linearized material behavior (Hsiung, et al., 2007). CNWRA staff also conducted additional two-dimensional (2D) analyses using both UDEC Version 5.0 (Itasca Consulting Group, 2011) and FLAC Version 5.0 (Itasca Consulting Group, 2005) codes to assess the spatial variation of the ground response at the surface.

This report documents the analysis conducted so far in estimating the ground motion at different locations at the surface when the seismic waves from a nearby strong motion earthquake, Coalinga1 (Hsiung, et al., 2007), propagate through the rock and soil layers. The rock and layers form a rock mass fractured by a number of faults and joint sets. Additionally, materials in all rock and soil layers sustain significant deterioration of the shear modulus (modulus of rigidity) when the waves propagate through them.

1.2 Objectives and Scope

The objectives of the analyses reported in this document are to assess the potential spatial variation of ground response at the surface when the seismic waves from the underlying bedrock propagate through a fractured and/or layered deposit with material variability and a thick soil cover. In addition, the shear modulus of these materials deteriorates when subjected to high shear strain from the propagating seismic waves. This report documents the results obtained from the analyses for understanding the phenomena that take place when these materials are subjected to large-amplitude seismic waves from a strong-motion earthquake. The analyses were conducted using various readily available data associated with the proposed geologic repository site at Yucca Mountain, Nevada. However, note that the results reported here are preliminary approximations and do not pertain to any licensing action; the geometry of the rock mass and, in some cases, material properties were significantly simplified for ease in analysis.

Behavior of soil and rock under dynamic load is discussed in Chapter 2. Traditional site response analysis is discussed in Chapter 3. Discussion also includes spatial variation and resonant behavior observed in the ground motion in 2D analyses and in actual earthquake records. Results obtained in this study using UDEC and FLAC codes are given in Chapter 4. Chapter 5 summarizes this study and discusses proposed future work.

2 DYNAMIC SOIL/ROCK BEHAVIOR

Generally, soils including soft rocks exhibit nonlinear response under shear loads especially at larger strain amplitudes. The shear modulus of the material decreases as the shear strain increases with an accompanying increase in material damping. These changes in material properties affect the amplitude and frequency content of the resulting ground motion. The constitutive model for the material response must account for these changes in the material properties to appropriately model the ground response.

It is well known that soil and rock exhibit nonlinear hysteresis behavior, as shown in Figure 2-1 (Kramer, 1996; Bechtel SAIC Company, LLC, 2004; EPRI, 1993). The inclination of the hysteresis loop is dependent on the soil stiffness and expressed by the tangent shear modulus G_{tan}. G_{tan} varies throughout the loading cycle, its average value over the loop is approximated by the secant shear modulus G_{sec}

$$G_{sec} = \frac{\tau_c}{\gamma_c} \tag{2-1}$$

where τ_c and γ_c are the magnitudes of shear stress and shear strain, respectively.

The breadth of the hysteresis loop represents the energy dissipated in a loading cycle and is described by the damping ratio ξ

$$\xi = \frac{1}{2\pi}\frac{A_{loop}}{G_{sec}\gamma_c^2} \tag{2-2}$$

where A_{loop} is the area of the hysteresis loop. G_{sec} and ξ are called the equivalent nonlinear material parameters of the soil.

Secant modulus G_{sec} of a soil varies with the cyclic shear strain amplitudes; at low shear strain, G_{sec} is large but it decreases as the strain amplitude increases. The secant modulus at zero cyclic shear strain amplitude has the highest value G_{max}. The secant modulus normalized by this highest value G_{max} as a function of the shear strain for tuff rock (Upper Mean Tuff) and alluvium (Upper Mean Alluvium) at the Yucca Mountain site is shown in Figure 2-2 (Bechtel SAIC Company, LLC, 2004) and is consistent with the typical curves observed for soils (EPRI, 1993).

Although there should not be any hysteretic dissipation of energy at strains below the linear cyclic threshold shear strain, experimental results do show some energy dissipation even at very low shear strain levels. The breadth of the hysteresis loops increases with the increasing cyclic shear strain amplitude indicating that the damping ratio increases with increasing strain amplitudes. Figure 2-3 (Bechtel SAIC Company, LLC, 2004) shows the variation of the damping ratio with strain amplitude for tuff and alluvium at the Yucca Mountain site.

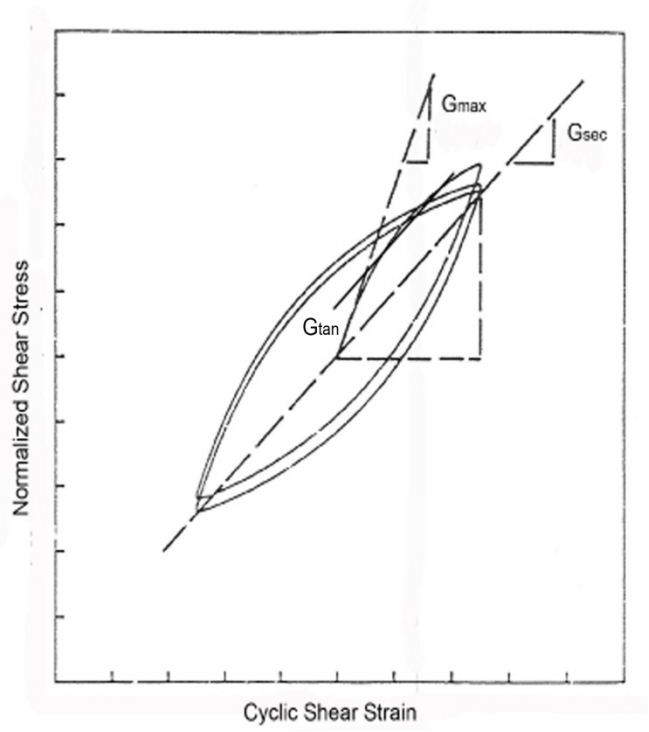

Figure 2-1. Typical Shear Stress and Shear Strain Relationship (Modified From Kramer, 1996)

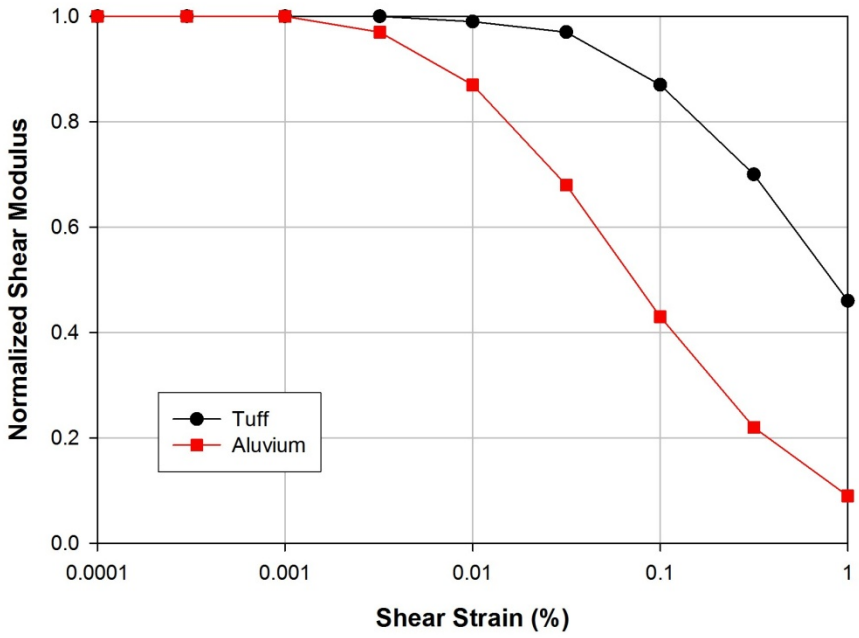

Figure 2-2. Variation of Normalized Shear Modulus With Shear Strain Using Data for Upper Mean Tuff and Upper Mean Alluvium From Bechtel SAIC Company, LLC (2004)

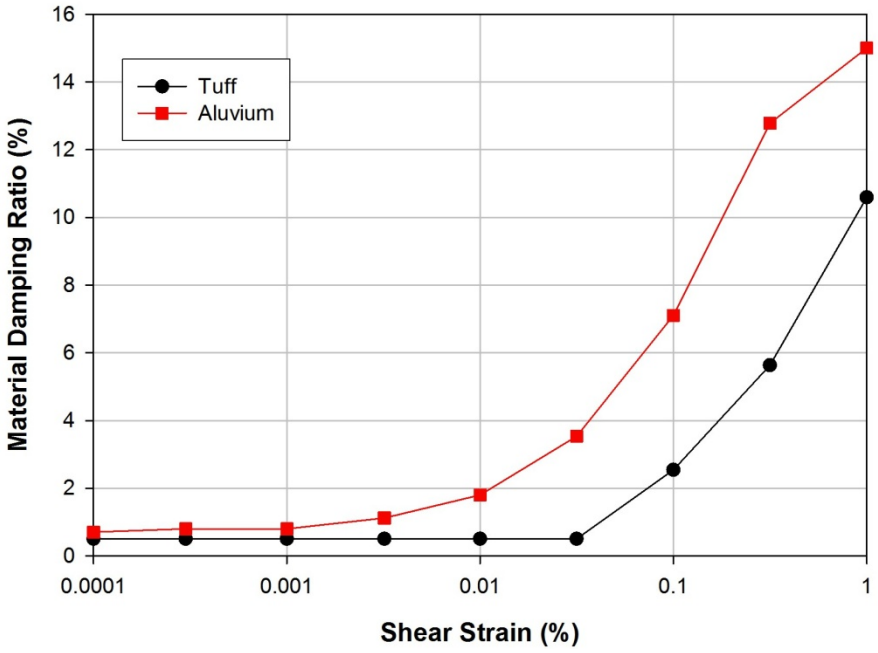

Figure 2-3. Variation of Material Damping Ratio With Shear Strain Using Data for Upper Mean Tuff and Upper Mean Alluvium From Bechtel SAIC Company, LLC (2004)

3 SITE RESPONSE ANALYSIS

1D ground response analyses assume that the medium above the bedrock is composed of horizontal strata and the ground response is predominantly due to the shear waves propagating vertically (Kramer, 1996). It is inherently assumed that the bedrock and the overlain strata are infinite in the horizontal direction.

In a linear approach to ground response analysis, transfer functions are used to estimate the response parameters, such as displacement, velocity, acceleration, shear stress, and shear strain, to an input motion, such as acceleration at the bedrock (Kramer, 1996), using the superposition principle. The transfer function is defined as the ratio of the seismic motion amplitude at the soil surface to the amplitude at the bedrock. SHAKE (Schnabel, et al., 1972) is the well-known computer program that implement the super position approach. The known ground motion at the bedrock is decomposed into a Fourier series (i.e., a series of sine waves with different amplitudes, frequencies, and phase angles), generally using the Fast Fourier Transform (FFT). The contribution of each Fourier component is estimated using the transfer function. Using the inverse FFT, the ground motion at the top surface is estimated (Kramer, 1996). Nonlinear behavior of the medium is generally approximated using an iterative procedure with equivalent linear properties (Kramer, 1996). As an alternative approach, the actual nonlinear response of a soil deposit can be analyzed using direct numerical integration in the time domain (Kramer, 1996). Currently available computer programs for nonlinear 1D ground response analysis represent the stress-strain behavior of the medium by different models (e.g., hyperbolic, modified hyperbolic, Ramberg-Osgood) (Kramer, 1996).

The equivalent linear approach is computationally simple and provides reasonable estimate of soil response subjected to seismic excitation in many situations; however, it is still an approximation to the nonlinear seismic ground response. The shear modulus and damping ratio would remain constant throughout the seismic excitation, although, as discussed later in this report, they are strongly dependent on the amplitude of shear strain (Arslan and Siyahi, 2006). The difference between the results from equivalent linear and nonlinear analyses is dependent on the degree of nonlinearity, as shown in Figure 2-2, of the medium response, in terms of degradation of rigidity modulus to dynamic load. For cases with high strain levels (i.e., shear stress approaches the shear strength of the medium), a nonlinear analysis is likely to produce reasonable results. On the other hand, both types of analyses are expected to produce reasonable results if the level of strain is low (i.e., stiff medium and/or weak input seismic motion) (Kramer, 1996). The differences in estimated ground response using linear and nonlinear approaches follow (Kramer, 1996; Arslan and Siyahi, 2006):

- An inherent linearity assumption may generate spurious resonance. As the stiffness of the medium decreases over the duration of large earthquakes, such high amplification levels will not develop in the field.

- Use of an effective shear strain in an equivalent linear analysis may lead to an oversoftened and overdamped system in cases where the peak shear strain is significantly larger than the remainder of the shear strain pulse. Alternatively, in cases with nearby uniform shear strain amplitude, it will develop an undersoftened, underdamped system.

- Nonlinear analysis requires an appropriate constitutive model; however, the parameters describing such models are generally not well established compared to the equivalent linear model. A substantial laboratory and field testing program is needed to appropriately evaluate the parameters characterizing the nonlinear stress-strain model.

1D analysis is appropriate for cases with horizontal strata or gently sloping sites with parallel material boundaries. If the strata are not horizontal, stiff materials are present, or materials with nonparallel boundaries are present, 2D and in some cases, 3D analysis will be required. In this study, a time domain (i.e., direct integration) method has been used to address the problem.

Site response assessment is typically conducted using 1D analysis assuming horizontally bedded strata with linear elastic material behavior. Many recent studies, however, have shown that 2D and 3D analyses may be required to fully capture the complexities in the subsurface, such as tilted layers and sedimentary basin effects (e.g., Bardet, et al., 1997, 1992; Frankel, 1993; Graves, 1993; Hartzell, et al., 1996; Zhang and Papageorgiou, 1996; Bielak, et al., 1999, 2003; Xu, et al., 2003; Yoshimura, et al., 2003). For example, Bardet, et al. (1992) analyzed the site response of the Marina District of San Francisco during the Loma Prieta earthquake. A nonlinear 1D analysis predicted a peak acceleration of 0.12 g at the ground surface in the Marina District with a bedrock peak acceleration of 0.067 g. The predicted ground surface motion is approximately 80 percent larger than the motion at the bedrock. SHAKE predicted a larger amplification because it uses an equivalent linear material model that does not consider complete failure. The 2D analyses predicted a peak ground acceleration of 0.20 g, approximately three times the amplification of the bedrock motion. Predicted larger peak accelerations with the 2D analyses indicate that the 1D site-response analyses used in traditional engineering practice may not necessarily be conservative.

Bielak, et al. (1999) compared results of 1D and 2D analyses for ground responses in an alluvial valley for the magnitude 6.8 earthquake in northern Armenia on December 7, 1988. Bielak, et al. (1999) made the following conclusions.

- The 1D amplification ratio exhibited the resonant behavior typical of a flat-layered system.

  The 2D amplification ratio exhibited resonant behavior in the vicinity of the 1D resonant frequencies; however, the corresponding 2D frequencies were slightly higher because of the lateral confinement the valley provided. The values of the respective peaks were considerably larger in the 2D simulations.

- The 2D amplification ratios greatly exceeded the 1D value. Interestingly, at certain frequencies the 2D amplification ratio was smaller than unity, indicating deamplification, or destructive interference of seismic waves.

4 ANALYSIS OF SURFACE RESPONSE

The software FLAC Version 5.0 (Itasca Consulting Group, 2005) and UDEC Version 5.0 (Itasca Consulting Group, 2011) have been used to simulate the waves propagating upward through the layered strata. FLAC is a 2D explicit finite difference program for engineering mechanics computation. Materials are represented by elements, or zones, which form a grid that the user adjusts to fit the shape of the object to be modeled. Each element behaves according to a prescribed linear or nonlinear stress-strain law in response to the applied forces or boundary restraints. The explicit, Lagrangian calculation scheme and the mixed-discretization zoning technique used in FLAC ensure that plastic collapse and flow are modeled accurately. UDEC is a 2D distinct element code that can simulate the response of a fractured rock mass subjected to dynamic loads. The medium is represented as an assemblage of discrete blocks. Large displacements are allowed along discontinuities between blocks. Rotation of individual blocks is allowed.

The recorded motion of the Coalinga1 earthquake with a 5×10^{-4} annual exceedance frequency, as used in Hsiung, et al. (2007), has been used in this study. This earthquake had a moment magnitude of 5.2 measured at the Transmitter Hill Station 10.4 km [6.5 mi] from the epicenter. The earthquake time history in terms of particle acceleration is shown in Figures 4-1 and is used in FLAC simulations. Figure 4-2 shows the time history in terms of particle velocity used in UDEC simulations. It should be noted that the amplitude of the particle velocity time history has been amplified to induce fracture opening and/or failure in the UDEC simulations. As the UDEC simulations assumed elastic behavior of the blocks, an increase of input motion amplitude will not cause any rock failure and, thereby, affect the resulting ground motion at the surface.

4.1 Fractured Rock Mass Model: UDEC Analysis

This analysis assesses the effects of the fractured rock mass on the propagating seismic waves. The rock mass is modeled to comprise many smaller sized rock blocks. Different types of fractures—namely, faults, layer contact boundaries, and joints—are assumed to exist in the rock mass. Large deformation of the rock mass as the seismic waves pass through would mostly be realized by the fractures. Currently available constitutive models for intact blocks and joints cannot simulate the degradation of shear modulus as a function of the shear strain, as shown in Figures 2-1 and 2-2.[1] Therefore, relative deformation between the blocks and the fractures would influence the propagation of the seismic waves and an inherent assumption in this analysis is that the shear strain in both rock and alluvium is small.

4.1.1 Rock Mass Model in UDEC

Figure 4-3 shows the fractured rock mass that has been modeled in this analysis using the UDEC code. An area where the proposed surface facilities of the geologic repository would be located was selected in this analysis because significant information has been collected for this

[1]Development of a material constitutive model in UDEC to represent degradation of shear modulus and damping ratio as a function of shear strain similar to that in the FLAC code is a major endeavor and is outside the scope of this activity.

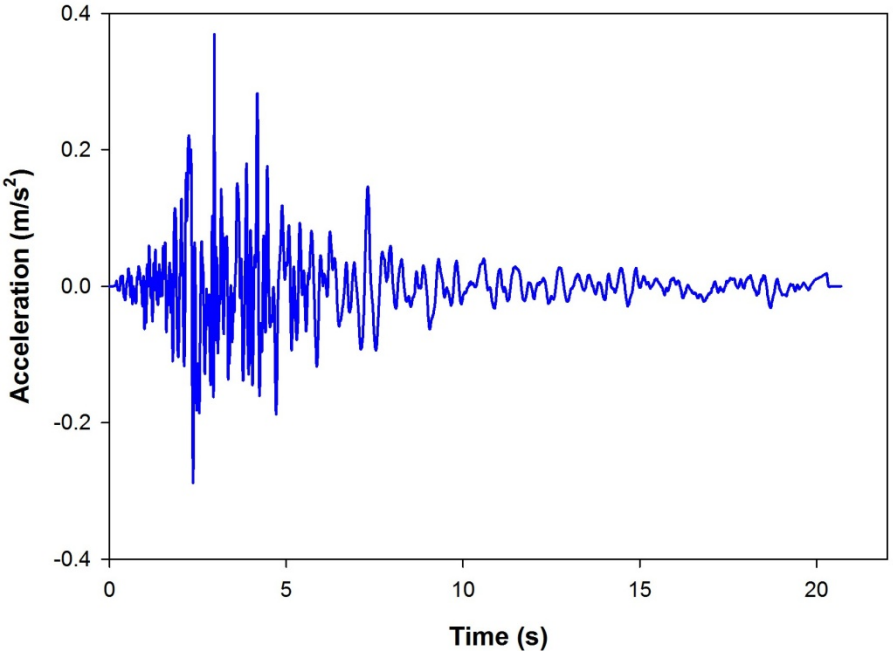

Figure 4-1. Particle Acceleration Versus Time of the Coalinga1 Earthquake Used in FLAC Simulations

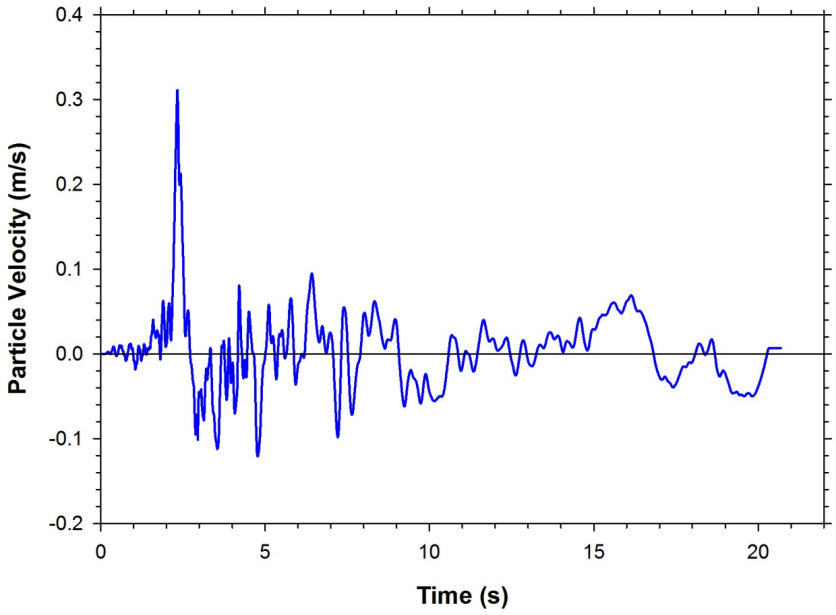

Figure 4-2. Input Motion in Terms of Particle Velocity Versus Time Used in UDEC Simulations

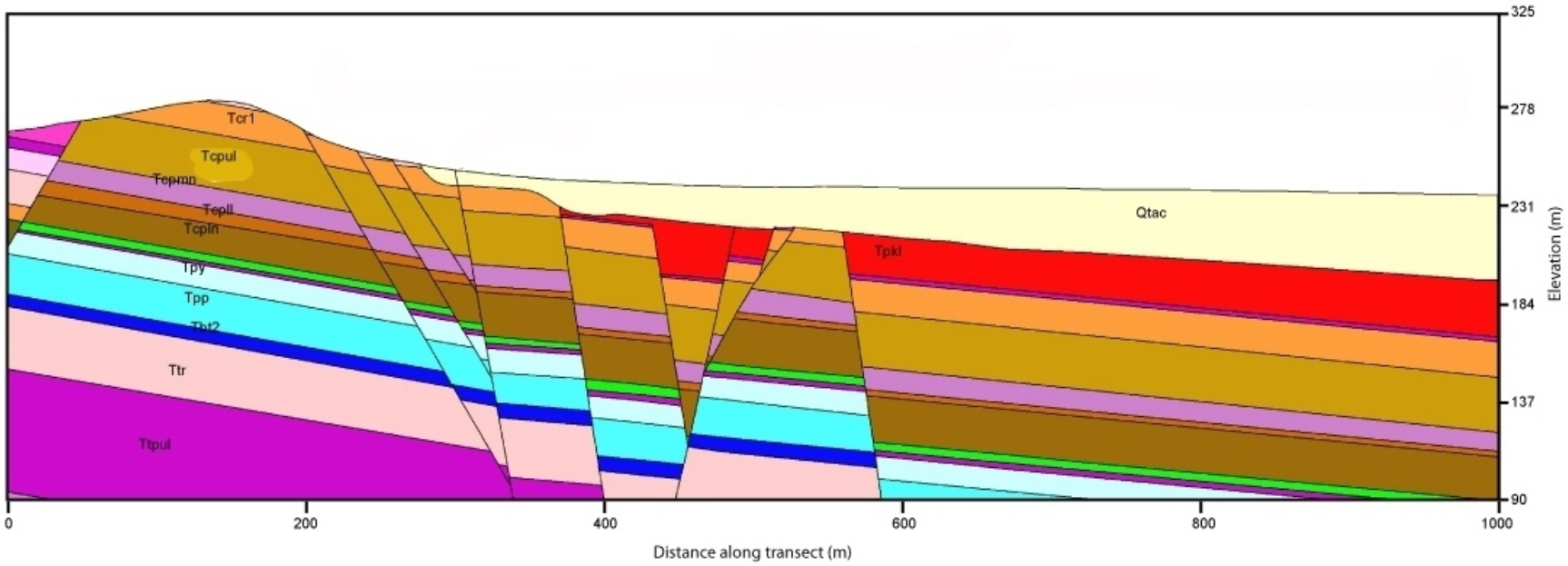

Figure 4-3. Cross Section of Strata Used in Seismic Response Modeling Using the UDEC Code (Description of Strata is given in Table 4-1)

area. Figure 4-3 shows the surface topography is not uniform and is reproduced in the UDEC model, as shown in Figure 4-4. The UDEC model is 600 m [1,969 ft] in length. It starts 50 m [164 ft] from the left side of Figure 4-3 and extends up to 650 m [2,134 ft] in the horizontal direction. The UDEC model extends to a depth of 200 m [656 ft] at one side and approximately 260 m [853 ft] at the other side due to presence of a small hill.

Additionally, in a few UDEC simulations, two joint sets are incorporated in the UDEC model in addition to the faults and strata layers shown in Figure 4-4. One set of joint dips toward the left at an angle of 30° with a spacing of 8 m [26 ft] and trace length of 30 m [98 ft]. There is a 2-m [6-6 ft] variation of spacing about the mean spacing value. Trace length has a variation of 10 m [33 ft] about the mean trace length value. Properties of faults and strata contacts are given in Table 4-1. Fracture properties used in different simulations are given in Table 4-2.

Property values used in both Tables 4-2 and 4-3 are within the range of rock fracture properties Hsiung, et al. (1994) observed for Apache Leap tuff joints.

Note that measured *in-situ* stiffness and strength properties of faults, in some cases with substantial thickness of gauge materials, are generally not available in the literature and are assumed to be within the measured properties of natural joints, both fresh (previously not sheared) and previously sheared with none to a small amount of gauge materials. The UDEC model has a zero horizontal velocity boundary condition at both lateral boundaries and a zero vertical velocity boundary condition at the bottom boundary. During simulation of wave propagation, the “free field” boundary condition is applied at both lateral boundaries. As UDEC requires a “quiet” boundary for application of the input seismic motion as particle velocity, the bottom boundary of the model is made of a “quiet” boundary. A Rayleigh damping of 5 percent of the critical damping, applied at the approximate natural frequency, was used in all simulations. The natural frequency of the model was estimated using the same model by suddenly applying the gravity load. The vertical velocity was measured at different points in the model. As the model is highly nonuniform with different types of fractures oriented at different directions and different types of materials with significantly different properties, the estimated frequency varies somewhat at different monitoring locations. An average frequency was used in these simulations.

UDEC solves a dynamic problem using an explicit time-marching scheme. In UDEC simulation, the timestep is dependent on the stiffness properties. The timestep UDEC estimated to solve these complex simulations was in the neighborhood of a fraction of a microsecond. Consequently, runtime required for simulating the effects of the first 25 seconds of the seismic signal would be at least a week for the available computer resources. Consequently, it was decided to run up to 5 seconds for each problem to complete several simulations in a reasonable time. Additionally, UDEC has an option to partially scale up the mass of the blocks to increase the speed of calculation. A partial mass scaling was used to achieve a timestep in the neighborhood of 50 microseconds.

Both frequency content and velocity of propagation of the input wave will affect the numerical accuracy of wave transmission. For accurate representation of wave transmission through a numerical model, the element (zone) size S should be

$$S \leq \frac{\lambda}{10} \tag{4-1}$$

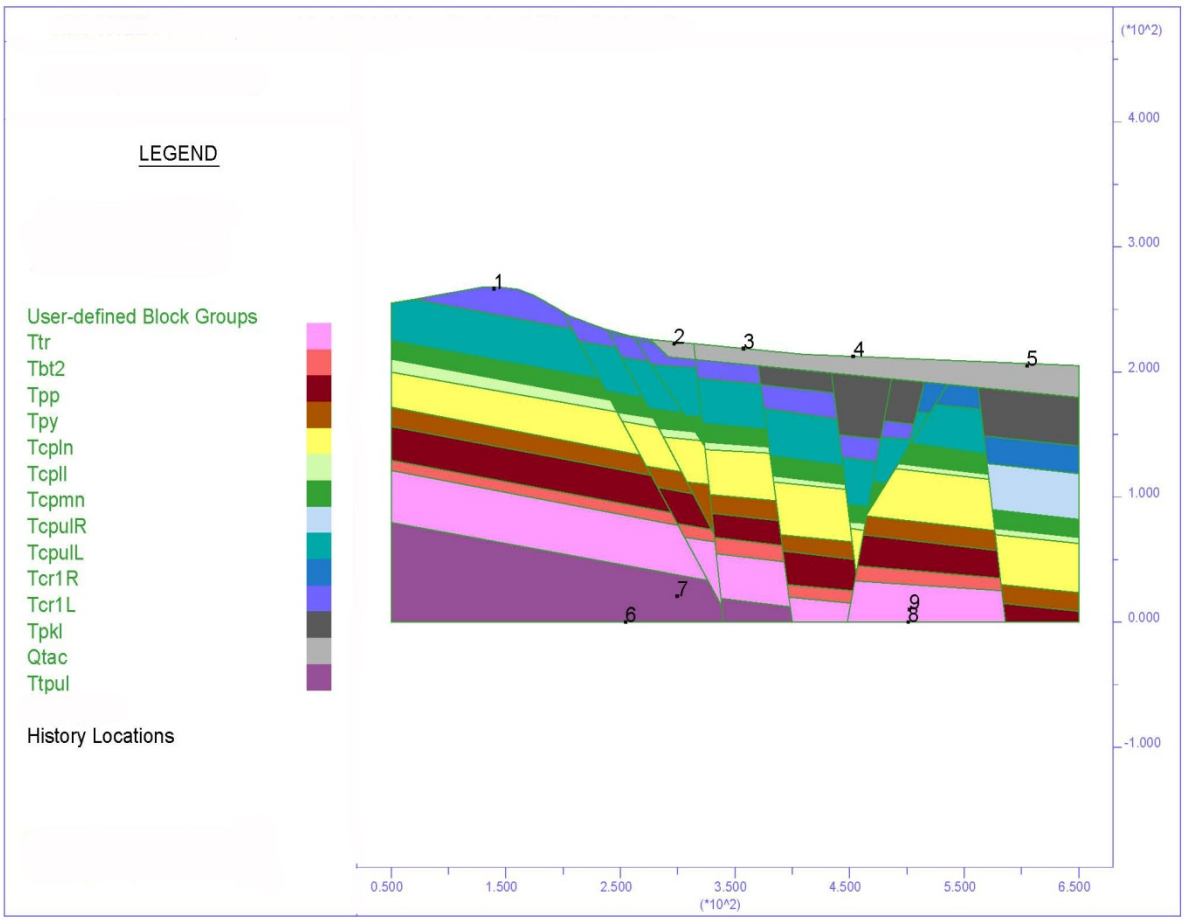

Figure 4-4. The UDEC Model of the Strata Cross Section With Monitoring Points 1–9. Monitoring Points 1–5 are on the Surface, Points 6 and 8 at the Bottom Boundary (on Bedrock), and Points 7 and 9 Inside the Model.

Table 4-1. Material Properties Used in UDEC Simulations

Unit	Description	Unit Weight	Shear Wave Velocity	Compression Wave Velocity	Shear Modulus (Pa)	Bulk Modulus (Pa)
Ttpul	Upper Lithophysal Zone of Crystal-Poor Member of Topopah Spring Tuff	2,200 kg/m^3 [137.3 pcf]	1,759 m/s [5,771 ft/s]	3,404 m/s [11,165 ft/s]	6.81×10^9	1.65×10^{10}
Ttr	Crystal-Rich Member of Topopah Spring Tuff	2,127 kg/m^3 [132.8 pcf]	1,978 m/s [6,490 ft/s]	3,228 m/s [10,591 ft/s]	8.32×10^9	1.11×10^{10}
Tbt2	Pre-Pah Canyon Tuff	1,000 kg/m^3 [62.4 pcf]	700 m/s [2,300 ft/s]	1,247 m/s [4,091 ft/s]	4.90×10^8	9.02×10^8
Tpp	Pah Canyon Tuff	1,200 kg/m^3 [74.9 pcf]	1,102 m/s [3,615 ft/s]	1,809 m/s [5,935 ft/s]	1.46×10^9	1.98×10^9
Tpy	Yucca Mountain Tuff	1,500 kg/m^3 [93.6 pcf]	1,230 m/s [4,035 ft/s]	2,011 m/s [6,598 ft/s]	2.27×10^9	3.04×10^9

Table 4-1. Material Properties Used in UDEC Simulations (continued)						
Unit	Description	Unit Weight	Shear Wave Velocity	Compression Wave Velocity	Shear Modulus (Pa)	Bulk Modulus (Pa)
Tcpln	Lower Nonlithophysial Zone of Tiva Canyon Tuff	2,127 kg/m^3 [132.8 pcf]	1,894 m/s [6,213 ft/s]	3,221 m/s [10,568 ft/s]	7.63×10^9	1.19×10^{10}
Tcpll	Lower Lithophysial Zone of Tiva Canyon Tuff	2,207 kg/m^3 [137.8 pcf]	1,639 m/s [5,378 ft/s]	3,107 m/s [10,194 ft/s]	5.93×10^9	1.34×10^{10}
Tcpmn	Middle Nonlithophysial Zone of Tiva Canyon Tuff	2,321 kg/m^3 [144.9 pcf]	1,583 m/s [5,193 ft/s]	3,062 m/s [10,046 ft/s]	5.82×10^9	1.40×10^{10}
Tcpul	Upper Lithophysial Zone of Tiva Canyon Tuff	2,070 kg/m^3 [129.2 pcf]	1,132 m/s [3,713 ft/s]	2,139 m/s [7,018 ft/s]	2.65×10^9	5.94×10^9
Tcr	Crystal-Rich Member of Tiva Canyon Tuff	1,158 kg/m^3 [72.3 pcf]	1,277 m/s [4,190 ft/s]	2,535 m/s [8,317 ft/s]	1.89×10^9	4.92×10^9
Tpkl	Tuff Unit "x"	1,572 kg/m^3 [113.4 pcf]	1,118 m/s [3,318 ft/s]	2,029 m/s [6,657 ft/s]	1.96×10^9	3.85×10^9
Qtac	Undifferentiated Quaternary/Tertiary Alluvial and Colluvial Deposit	1,852 kg/m^3 [115.6 pcf]	712 m/s [2,336 ft/s]	1,485 m/s [4,872 ft/s]	9.40×10^8	2.83×10^9

Table 4-2. Properties of Faults and Strata Contacts Used in UDEC Simulations								
	Faults				Strata Contacts			
Case Number	1	2	3	4	1	2	3	4
Normal Stiffness k_n [GPa/m]	20	40	10	50	20	40	10	50
Shear Stiffness k_s [GPa/m]	10	20	5	30	10	20	5	30
Friction Angle φ [degree]	30	30	10	15	30	30	20	30
Cohesion C [MPa]	1	1	0.001	1	1	1	0.001	1

Table 4-3. Properties of Joints Used in UDEC Simulations (Case 4)		
	Left Dipping	Right Dipping
Normal Stiffness k_n [GPa/m]	50	50
Shear Stiffness k_s [GPa/m]	30	30
Friction Angle φ [degree]	30	30
Cohesion C [MPa]	1	1

where λ is the wave length associated with the highest frequency component of the input wave. Hsiung, et al. (2007, Table 2-3) show that the maximum shear velocity occurs for the case of "mean + one standard deviation" of Lower Nonlithophysal Tiva Canyon rock. It is 2,260 m/s [7,415 ft/s]. Therefore, the wavelength associated with the wave having frequency f is 2260/ f . For a maximum frequency of interest $f = 50$ Hz, the associated wavelength is 45 m [148 ft]. Consequently, the finite difference grid size in accordance with Eq. (4-1) should be less than or equal to 4.5 [15.6 ft] for a wave with frequency of 50 Hz to propagate adequately. The zone size in this model is smaller than 4.5 m [15.6 ft] for appropriate transmission of the input seismic waves applied at the base.

4.1.1.1 Results and Discussion

Locations of the monitoring points in the UDEC model are shown in Figure 4-4. Point 1 is on the top of the hill and is located on the rock layer. Points 2 through 5 are on the alluvium. The thickness of the alluvium layer is smallest at Point 2. It increases to the maximum at Point 5. Points 6 and 8 are at the bottom model boundary, which is assumed to be the top surface of the bedrock, and thereby show the seismic motion applied at the bottom boundary of the model. Points 7 and 9 are a small distance away: 20 m [66 ft] and 10 m [33 ft], respectively.

Models Fractured Rock Mass Only

Case 1: Fault Properties (k_n = 20 GPa/m, k_s = 10 GPa/m, φ = 30°, C = 1 MPa)
Contact Properties (k_n = 20 GPa/m, k_s = 10 GPa/m, φ = 30°, C = 1 MPa)

This case represents a typical scenario expected in nature. Both types of fractures have average stiffness and frictional strength properties and are well within the range observed (e.g., Hsiung, et al., 1994). It has been assumed that these fractures do not have any tensile strength, a generally conservative assumption. Figure 4-5 compares the particle velocity estimated at Point 1 with respect to the input motion for an analysis conducted for the first 5 seconds of the earthquake motion signal. The seismic motion after traveling through different layers is amplified as it passes through Point 1; the amplification is approximately 1.4, and peak amplitude is 0.43 m/s [1.41 ft/s] compared to 0.31 m/s [1.02 ft/s] of the input motion. Additionally, the shift observed in the time-varying signal is due to the finite propagation velocity of the seismic motion through different layers. Amplification of the seismic motion increases as the soil thickness increases. The soil thickness is maximum at Point 5, and the peak amplitude is 0.45 m/s [1.48 ft/s], an amplification approximately 1.5 times the input motion and approximately 7 percent higher than at Point 1. Figure 4-6 compares the amplification of seismic motion at Points 1 through 5 relative to the input motion at Point 6. Figures 4-5 and 4-6 show that individual pulses of the input seismic motion did not appreciably change shape as the waves propagate upward, when an elastic model without any damage parameter to represent the shear modulus and damping ratio degradation as a function of the shear strain was used in this analysis. Consequently, the seismic amplification estimated at the surface is smaller than in reality, where rigidity modulus degradation of the material may enhance the amplification of the seismic motion at the surface. UDEC results also show minor opening {approximately 0.6 mm [0.24 in]} of a strata contact near the surface. These results are compared with those from other cases in Table 4-4.

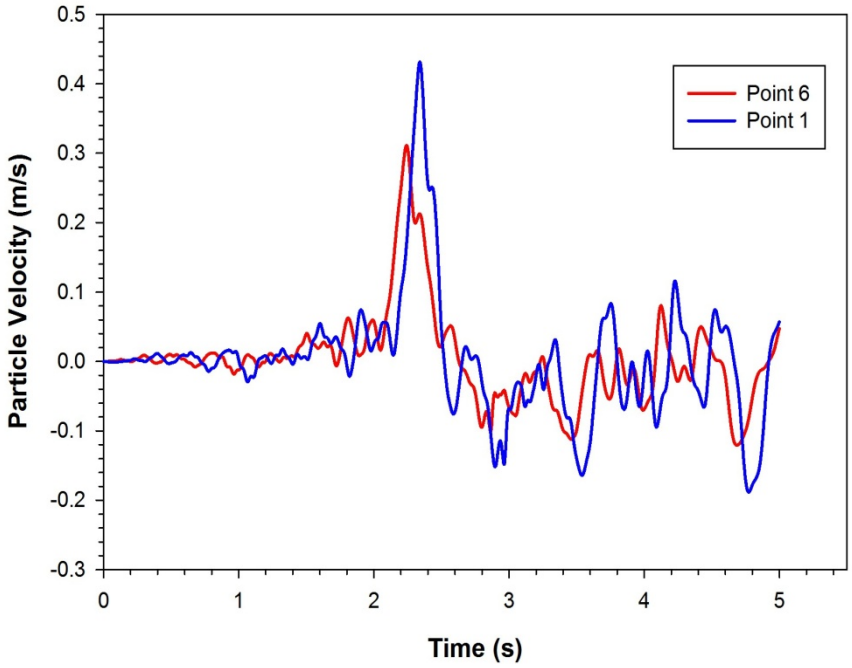

Figure 4-5. Comparison of Ground Motion at Point 1 With Input Motion (Point 6) (Case 1)

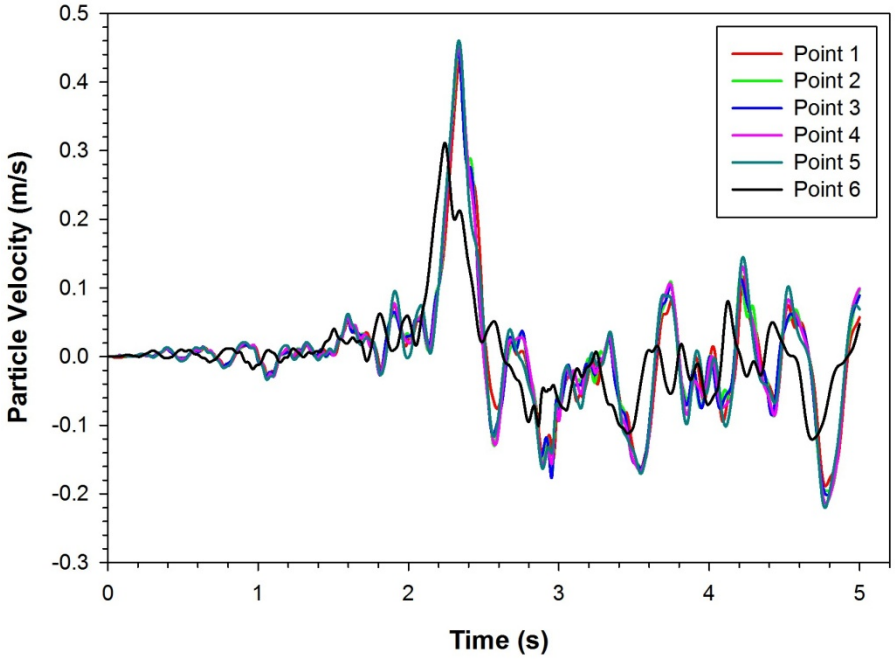

Figure 4-6. Comparison of Ground Motion at Points 1–5 With Input (Point 6) (Case 2)

Table 4-4. Results From Four Simulations Using UDEC			
Case	**Amplification**		**Comments**
	Peak Value	Percentage of Input	
1	0.43 m/s [1.41 ft/s]	140	Amplification is approximately 7 percent higher at Point 5, which is over the deepest part of the soil layer.
2	0.35 m/s [1.15 ft/s]	113	Significantly stiffer fracture planes resulting in an overall stiffener rock mass.
3	0.49 m/s [1.61 ft/s]	160	Significantly softer fracture planes resulting in an overall softer rock mass
4	0.49 m/s [1.61 ft/s]	160	Rock mass has two sets of joints; however, the fracture planes and joints are significantly stiffer.

Case 2: Fault Properties (k_n = 40 GPa/m, k_s = 20 GPa/m, φ = 30°, C = 1 MPa)
Contact Properties (k_n = 40 GPa/m, k_s = 20 GPa/m, φ = 30°, C = 1 MPa)

This case also may be a typical one in nature. Both normal and shear stiffness values are well within the range observed (e.g., Hsiung, et al., 1994). As the stiffness properties of both faults and strata contact planes increase, the timesteps required to complete 5 seconds of the Coalinga1 earthquake motion increases. Figure 4-7 compares the estimated seismic motion at the surface (Points 1–5) when the seismic motion is applied at the model base.

The peak amplitude of the seismic motion at Point 1 is approximately 0.35 m/s [1.15 ft/s], an amplification of 1.13 times of the input motion. The amplitude at Point 5 is 0.39 m/s [1.28 ft/s], an amplification of approximately 1.30 times. Reduction of the amplification magnitude compared to Case 1 can be attributed to the stiffer fracture planes, which make the rock mass stiffer overall. The time shift of the pulse at the top surface compared to the pulse applied at the base is smaller compared to that observed in Case 1, which has a less stiff rock mass. Again, the seismic pulses do not undergo any significant distortions, because an elastic model with no material degradation parameter has been assumed in the constitutive model for the rock blocks in this case. Results are provided in Table 4-4 for comparing with other cases.

Case 3: Fault Properties (k_n = 10 GPa/m; k_s = 5 GPa/m, φ = 10°, C = 0.001 MPa)
Contact Properties (k_n = 5 GPa/m, k_s = 5 GPa/m, φ = 20°, C = 0.001 MPa

This case may represent a scenario with low-end stiffness and strength values for both faults and strata contact planes; both faults and strata contact planes are assumed to be weak. Contact planes are assumed somewhat stronger than the fault planes. The amplification of the seismic motion at all points increases to approximately 1.6 times the input motion and the estimated amplitude is 0.49 m/s [1.61 ft/s], as shown in Figure 4-8. However, the difference between amplifications at Points 1 and 5 is small, less than 5 percent. Low stiffness of the faults and contact planes made the medium relatively soft, and, consequently, it can undergo larger deformation. Figure 4-8 also shows that transmission of seismic waves did not introduce distortion to the pulse shape; the materials did not degrade because elastic behavior of the materials was assumed. Information in Table 4-4 compares the results with those from other cases analyzed.

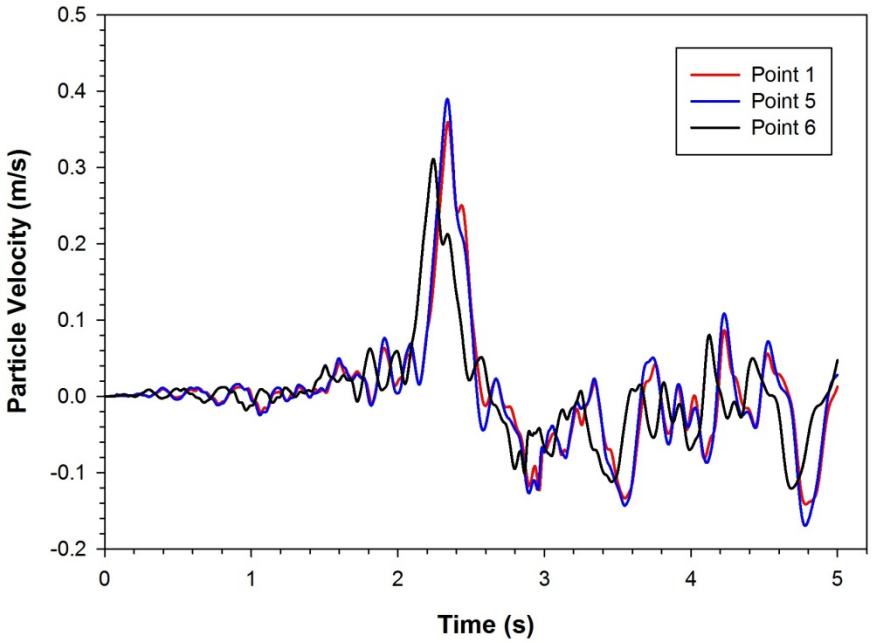

Figure 4-7. Comparison of Ground Motion at Points 1 and 5 with Input (Point 6) (Case 2)

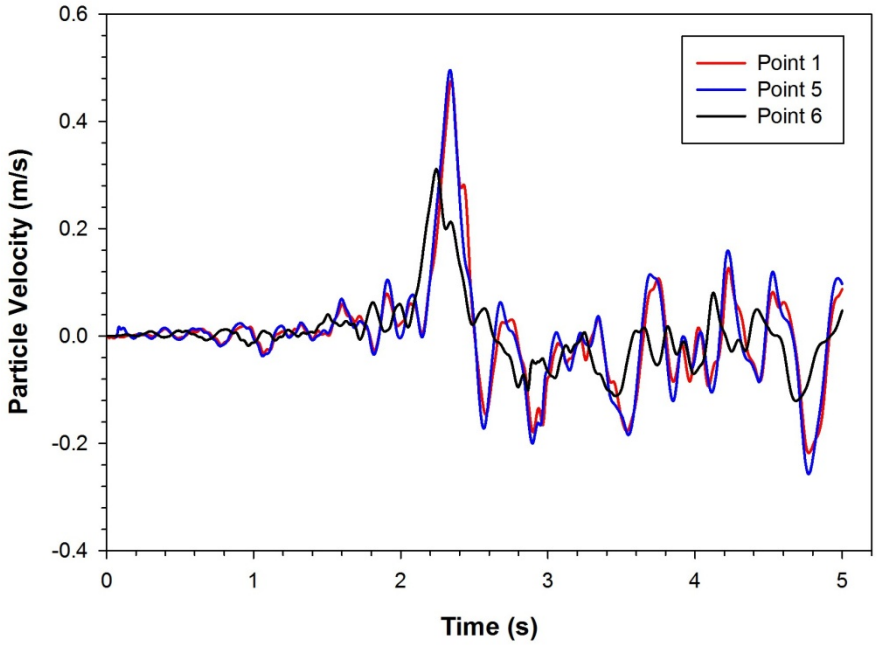

Figure 4-8. Comparison of Ground Motion at Points 1 and 5 With Input (Point 6) (Case 3)

Case 4: Fault Properties (k_n = 50 GPa/m; k_s = 50 GPa/m, φ = 15°, C = 1 MPa)
Contact Properties (k_n = 50 GPa/m, k_s = 30 GPa/m, φ = 15°, C = 1 MPa)
Joint Properties (k_n = 50 GPa/m, k_s = 30 GPA/m, φ = 30°, C = 1 MPa)

In this case, two sets of joints were incorporated into the rock mass model of faults and strata contact planes, as shown in Figure 4-9. One set of joints dips toward the left, and the other set dips toward the right. These additional fractures split each block into several small-sized blocks and make the model complex. The number of intersecting fractures and resulting blocks increases several fold. Tracking movement of these blocks in each calculation timestep adds significant bookkeeping tasks in UDEC runs. Consequently, this simulation model in UDEC will run significantly slower. The runtime for the input motion (Coalinga1 earthquake) up to 5 seconds took several days. Consequently, only one case could be successfully analyzed. Adding joints into the rock mass makes the overall material less stiff, which decreased the estimated average natural frequency to approximately 15 Hz. Figure 4-10 shows the estimated wave motion at Point 5 (on soil) compared to the input motion. The peak amplitude at Point 5 is 0.49 m/s [1.61 ft/s] compared to an input of 0.31 m/s [1.02 ft/s], approximately 1.6 times amplification. All measuring points on the surface (Points 1–5) recorded higher magnification of the seismic waves than the cases with no joints. As discussed, joints made the overall stiffness of the medium softer resulting in more deformation (as well as larger particle velocity) at the surface. Results are presented in Table 4-4.

4.2 Horizontal and Inclined Strata Models: FLAC Analysis

Two models were developed to assess the effects of inclined strata on the ground response to be realized on the surface as a result of seismic excitation at the base. The first model is composed of horizontal strata, and the second model has the same material layers dipping to the right. The difference in ground response between these two models would be due to inclined strata: the longer path to be traversed by the vertically propagating waves. The models are shown in Figures 4-11 and 4-12.

4.2.1 Strata Model

In this analysis, the material properties of the strata are assumed to be those of rock and alluvium at the Yucca Mountain site because the material properties data, especially the reduction of shear modulus with increasing shear strain, are readily available for this region (Bechtel SAIC Company, LLC, 2004). However, note that the analysis assumes a somewhat arbitrary thickness for each layer, which does not necessarily conform to strata thicknesses at the Yucca Mountain site. The material properties assumed for each stratum are given in Table 4-1. The grid size in the FLAC models was smaller than necessary to transmit waves with a frequency of 20 Hz.

The free-field boundary condition, available in FLAC, was used to simulate the infinite extent of the rock mass in the horizontal direction. This boundary condition accounts for the free-field motion that would exist in the subsurface strata in the absence of the “artificial” model boundaries as the input seismic waves propagate upward. This boundary condition not only allows placing the model boundaries sufficiently close resulting in a small-sized model, but also makes the boundaries nonreflecting. Plane waves, while propagating upward, suffer no distortion at the boundary as the free-field boundary; they are modeled as a 1D grid attached to the main grid representing the medium, supplying identical conditions of a model having infinite extent. As this boundary condition requires the model to be in static equilibrium, the model is

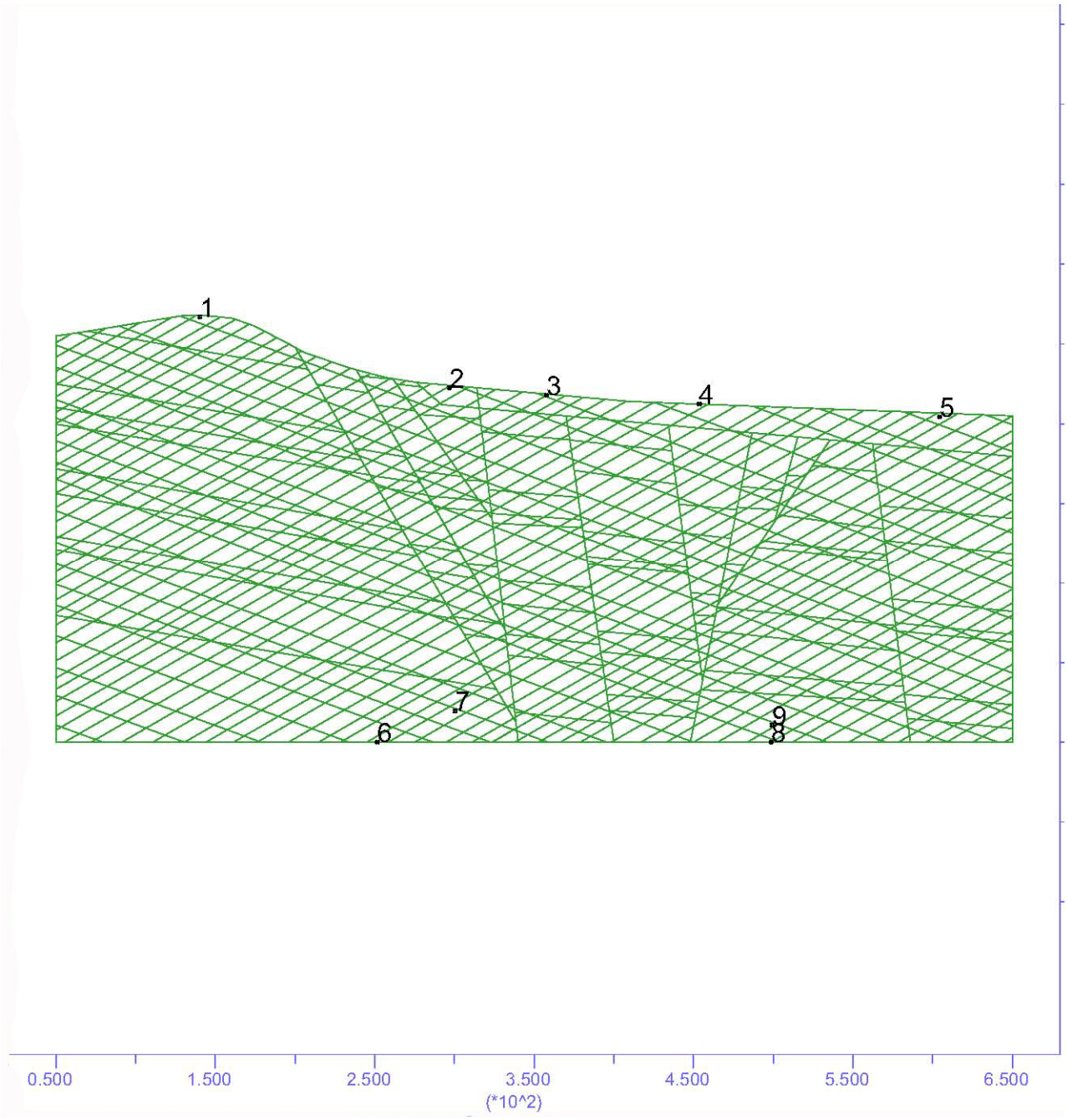

Figure 4-9. UDEC Model of the Fractured and Jointed Rock Mass; One Fracture Set Dips Toward the Left and Another Toward the Right

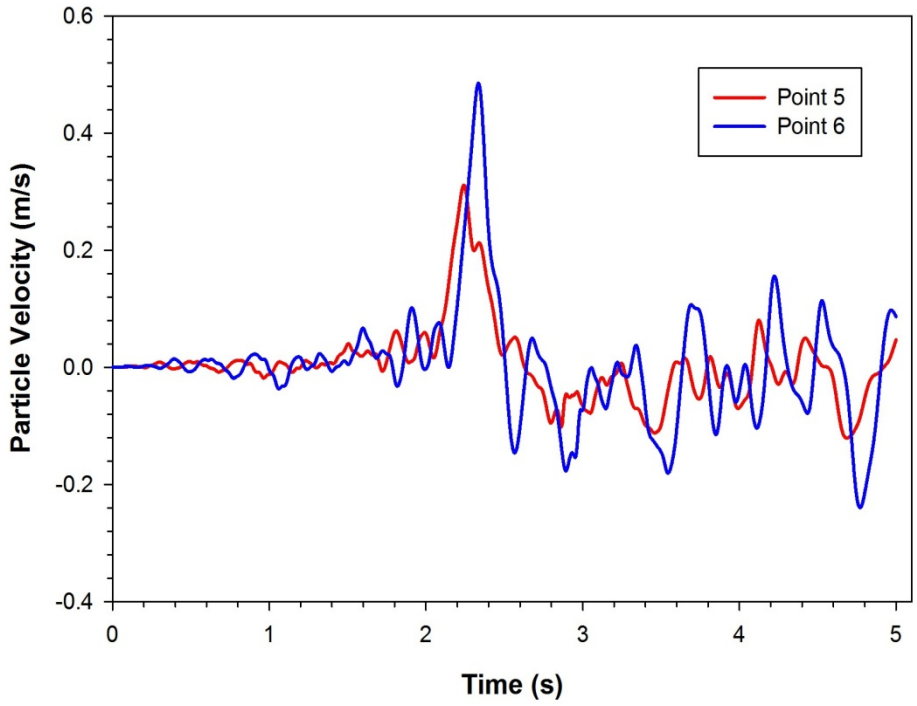

Figure 4-10. Comparison of Ground Motion at Point 5 (on Soil) With Input (Point 6) (Case 4)

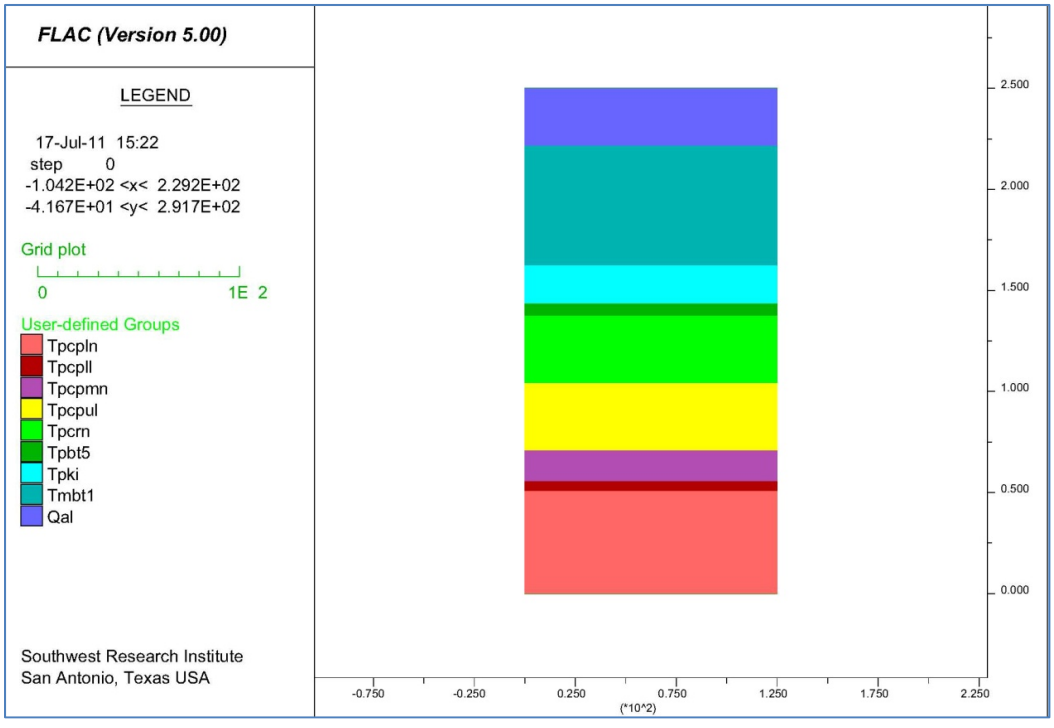

Figure 4-11. Horizontal Strata Model Used in FLAC Analysis

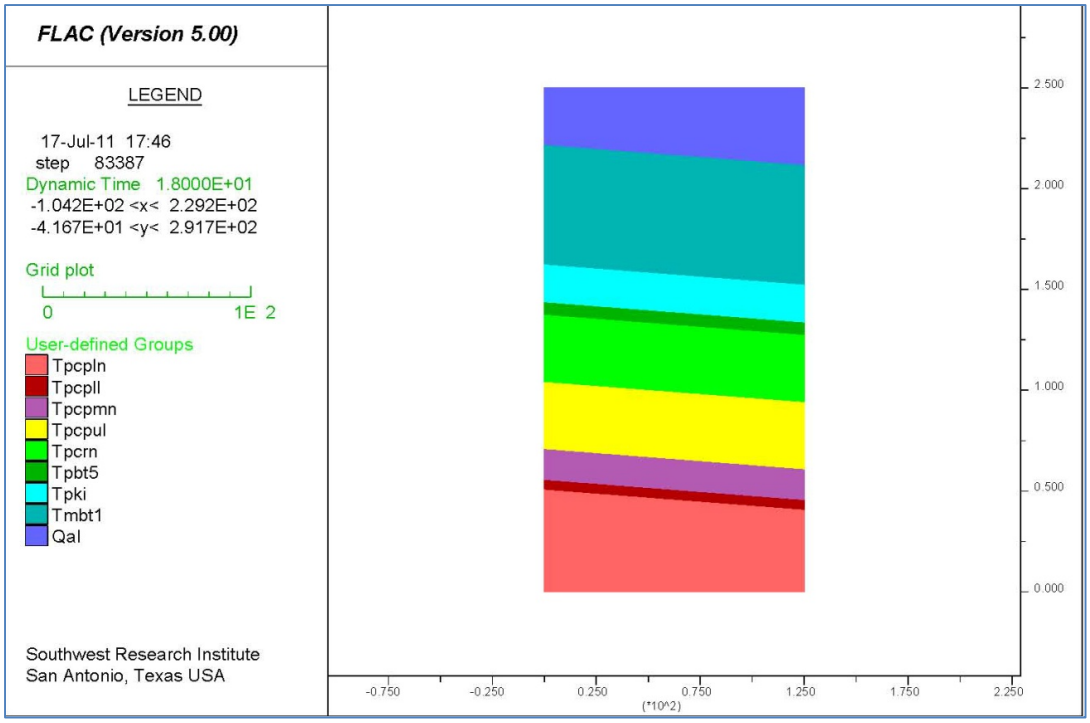

Figure 4-12. Inclined Strata Model Used in FLAC Analysis

first cycled 20,000 calculation steps with only gravity load to keep the unbalanced force in the model negligible. This state of model was used as the initial condition for propagating the seismic motion. The seismic motion of the Coalinga1 earthquake is applied at the bottom boundary as a table of discrete values of particle acceleration.

4.2.2 Model With Horizontal Strata Layers

In these simulations, the strata used are composed of horizontal layers, as shown in Figure 4-11. A grid of 50 horizontal and 200 vertical units was used to represent a block of materials 250 × 250 m [820 × 820 ft]. The materials deform as the seismic waves pass through and sustain damage in terms of degradation of rigidity modulus, as shown in Figures 2-2 and 2-3.

Reduction of normalized shear modulus and material damping ratio with shear strain has been represented by three different models available in FLAC and used in this analysis: (i) default, (ii) Sig3, and (iii) Sig4. Information for both tuff (Upper Mean Tuff) and alluvium (Upper Mean Alluvium) from Bechtel SAIC Company, LLC (2004) was fitted to these models. Bechtel SAIC Company, LLC (2004) combined results of laboratory tests of all tuff rocks as one material. In this study, the same degradation model parameters were used for all tuff layers. Results of fitting are discussed in the appendix. The fitted parameters are given in Tables 4-5 through 4-7.

Default Material Degradation Model

Figure 4-13 shows the estimated velocity history at the top surface. As this is a horizontal strata model, there is no spatial variation of the velocity (as well as acceleration) history at the base and the top surface. Figure 4-14 compares the input acceleration at the base and the top surface. The acceleration input at the base with peak amplitude of 0.37 m/s^2, as shown in

Table 4-5. Fitted Parameters for Default Model Representing Material Degradation With Shear Strain		
	Tuff	**Alluvium**
L_1	−3.425	−3.425
L_2	3.23	0.823

Table 4-6. Fitted Parameters for Sig3 Model Representing Material Degradation With Shear Strain		
	Tuff	**Alluvium**
a	0.997	1.012
b	−0.3034	−0.4753
x_0	−0.2334	−1.1418

Table 4-7. Fitted Parameters for Sig4 Model Representing Material Degradation With Shear Strain		
	Tuff	**Alluvium**
a	341.99	1.0217
b	−0.5125	−0.4837
x_0	3.227	−1.1322
y_0	−340.9961	-8.08×10^{-3}

Figure 4-1, amplifies by approximately 3.4 m/s^2 peak acceleration at the top of material column, almost 9 times amplification. Note in Figure 4-14 that the first major pulse of the input motion corresponds with a relatively large amplitude response followed by several large amplitude responses with similar amplitudes. It seems the first major pulse of the input motion degrades the rigidity modulus of the material significantly. This degradation is permanent. Input pulses that follow this first major pulse generate a significantly large response of the degraded materials.

The vibration at the top continues for a long time even after the input motion has died down. This is expected as the materials will continue to vibrate for some time. Note that the simulation only captured the first 20 seconds of the input motion. As a result, the trailing end of the surfaceground motion was not calculated. Although pseudo-acceleration response spectra, shown in Figure 4-15, have a peak around 1.2 Hz, other peaks occur at 3, 5, and 8 Hz.

Sig3 Material Degradation Model

Figure 4-16 compares the estimated horizontal acceleration at the surface with the input motion at the base. Input acceleration at the base is amplified to 3.4 m/s^2 peak acceleration, approximately nine times amplification, as the waves propagate upward. Like the previous case with the default model simulating degradation of material rigidity this model also shows peak pulse at the surface occurring at much later than the peak pulse of the input motion. The top surface seems to vibrate for a long time after cessation of a ground acceleration pulse containing significant energy.

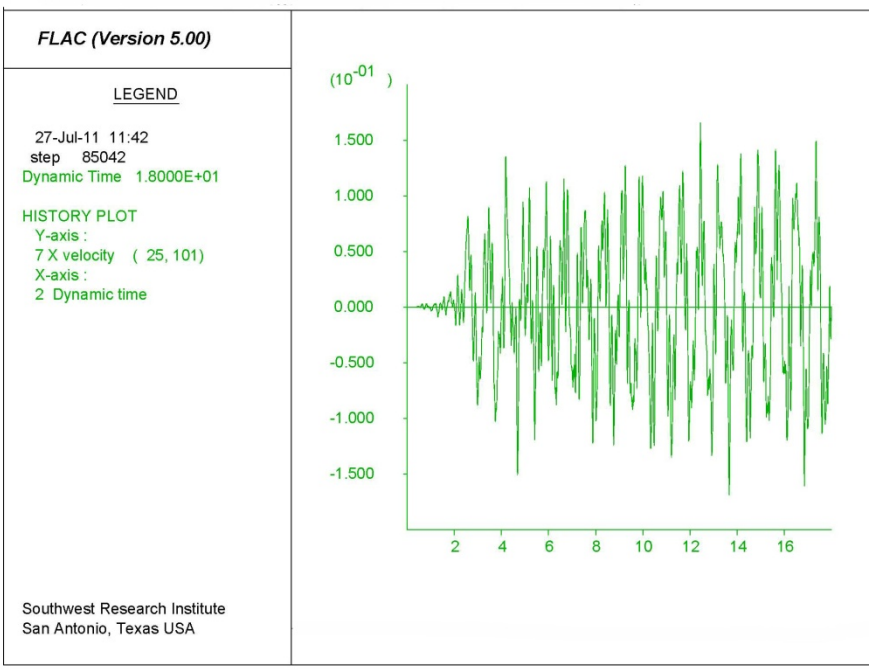

Figure 4-13. Estimated Velocity History at the Top of the Model for First 18 Seconds With the Default Material Degradation Model [y-axis: Velocity (m/s), x-axis: Time (s)]

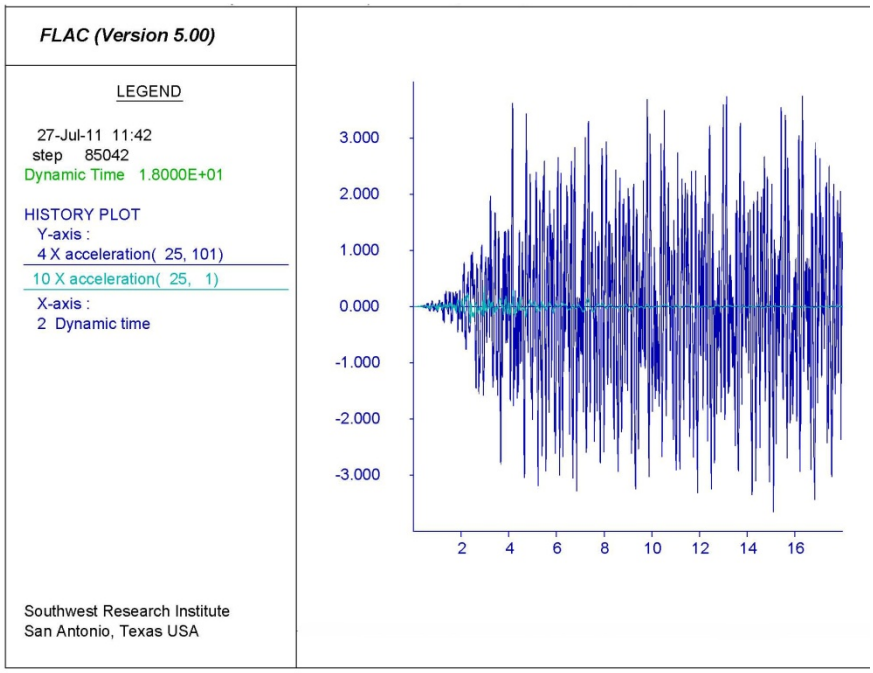

Figure 4-14. Comparison of Acceleration at the Top of the Model With Input Motion at the Base With the Default Material Degradation Model [y-axis: Acceleration (m/s^2), x-axis: Time (s)]

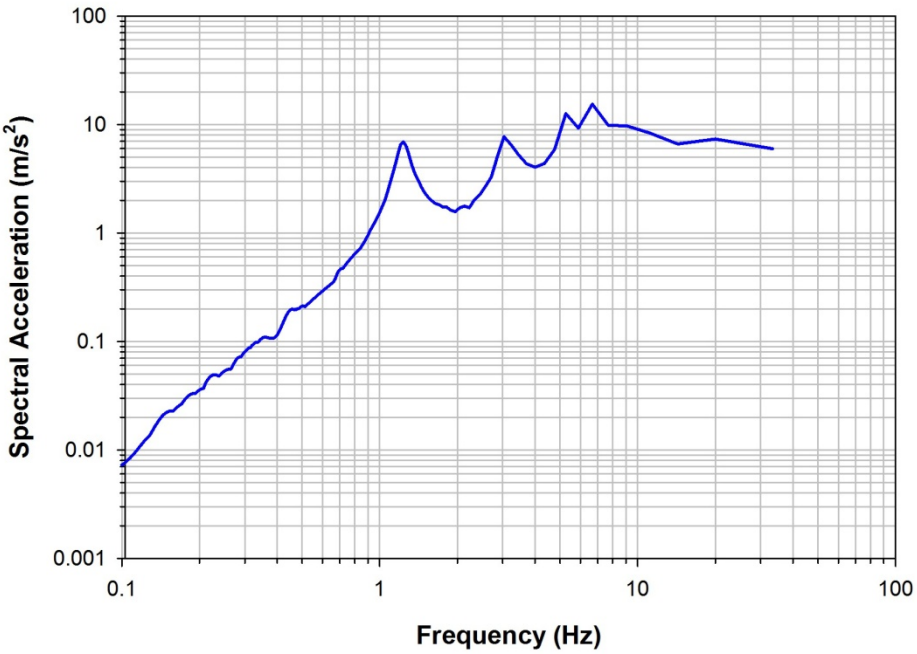

Figure 4-15. Spectral Acceleration at the Top Surface of the Horizontal Layer Model as a Function of Frequency

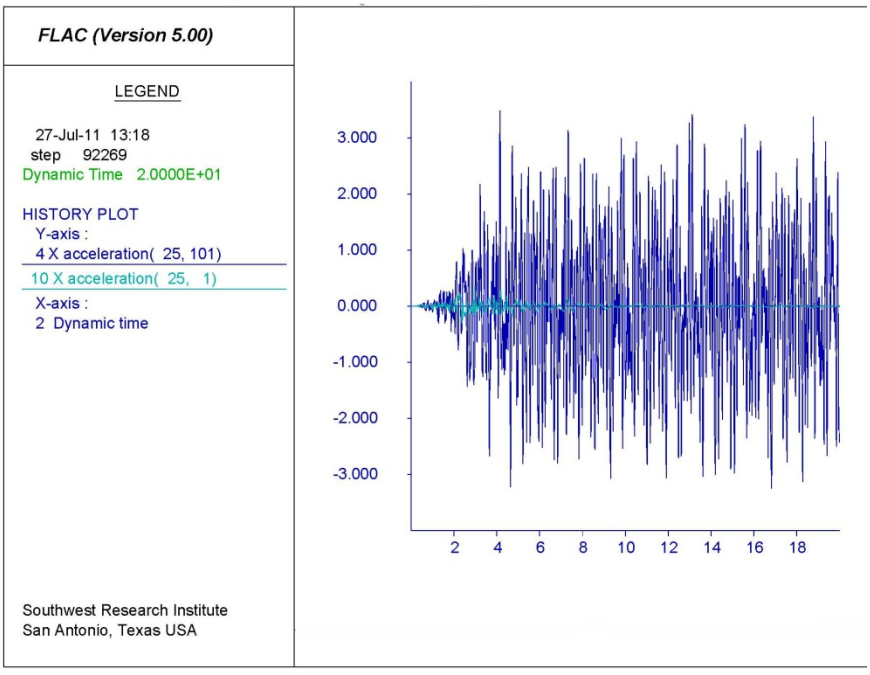

Figure 4-16. Comparison of Acceleration at the Top Surface with Input Motion at the Base With Sig3 Material Degradation Model [y-axis: Acceleration (m/s^2), x-axis: Time (s)]

Sig4 Material Degradation Model

Figure 4-17 compares the estimated horizontal acceleration at the surface of the material column with the input ground acceleration at the base. The input acceleration is significantly amplified at the top the estimated peak acceleration is almost nine times the input motion. The amplification is extremely high even at 18 seconds after the start of the seismic motion.

4.2.3 Model With Inclined Strata Layers

In this simulation, the strata layers dip toward the right (e.g., a limb of a fold structure), as shown in Figure 4-12. Material degradation increases with increase in shear strain, as shown in Figures 2-2 and 2-3. It is expected that the spatial variation of acceleration measured at the surface would be due to different materials encountered at different locations. Reduction of normalized shear modulus and material damping ratio with shear strain has been represented by the default model only in this analysis.

Figure 4-18 shows the variation of estimated horizontal acceleration at different locations on the surface. The input acceleration is amplified to an estimated peak acceleration of 3.5 m/s^2, and amplification of approximately 9.5 times the input motion. The top surface vibrates for a considerably longer time. Although not markedly different in these simulation result shown in Figure 4-18, the amplification increases to the right side of the model, where the thickness of the alluvium top layer increases continuously.

4.2.4 Basin Model: FLAC Analysis

As Bielak, et al. (1999) observed, the impedance contrast between the soil and rock layers, especially in a valley or basin-type deposit, controls the amplification of the input ground motion as the waves propagate to the surface. A higher contrast ratio produces larger amplification. In this analysis, a simple basin model has been developed to analyze the phenomena. The model is shown in Figure 4-19: a basin of relatively softer material (e.g., a soil deposit) is surrounded by a stiffer material (e.g., a rock deposit). All three rock types have the same material properties and, therefore, belong to the same rock unit.

The model is 500 m [1,640 ft] long and has a depth of 250 m [820 ft]. The soil basin is in the middle and has a length of 300 m [984 ft] with a depth of 150 m [492 ft]. The material properties used are given in Table 4-8 (QTac for soil and Tcpln for rock). Hysteretic damping of both soil and rock is represented by the default model available in FLAC with parameters, as given in Table 4-4. The impedance ratios between rock and soil used in these simulations are given in Table 4-9.

Figures 4-20 and 4-21 show the amplification of the input seismic motion in the large soil basin with an impedance ratio (Z_{Rock}/Z_{Soil}) of 5.0. Amplification is not uniform across the soil basin. Amplification increases toward the center of the basin and reaches maximum at the center. This phenomenon is present in all three cases analyzed here. Amplification also increases as the impedance ratio increases between the rock and soil, as can be seen in Figures 4-22 through 4-24 for three cases with increasing impedance ratio.

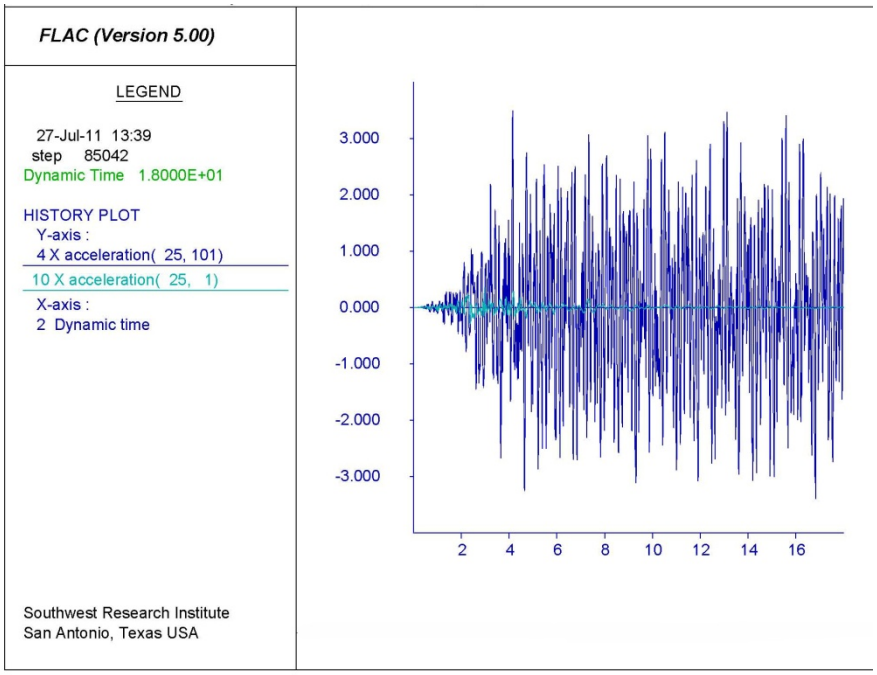

Figure 4-17. Comparison of Acceleration at the Top Surface With Input Motion at the Base With Sig4 Material Degradation Model [y-axis: Acceleration (m/s^2), x-axis: Time (s)]

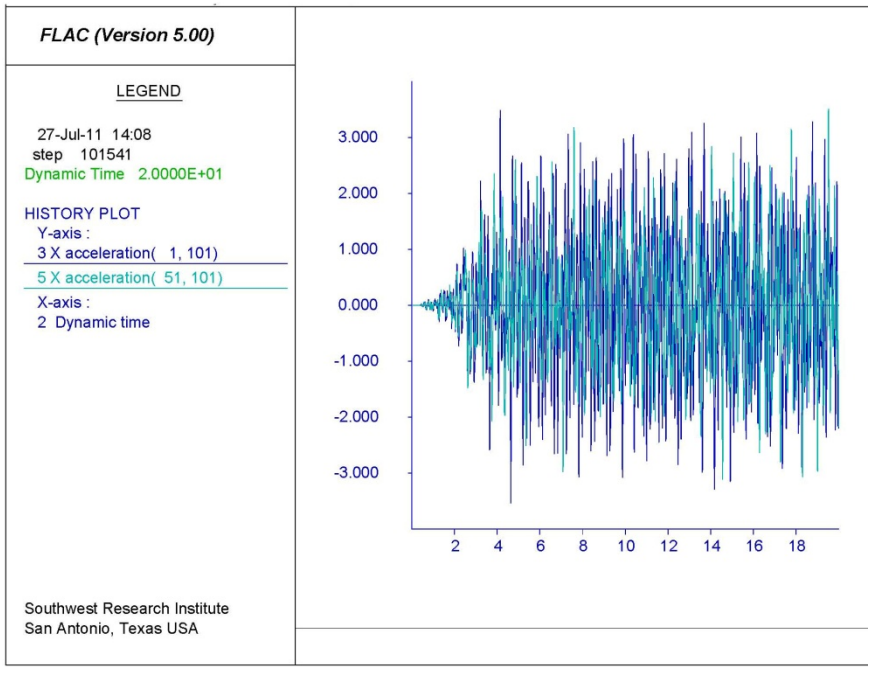

Figure 4-18. Comparison of Acceleration Time Histories at Left and Right Corners of the Inclined Strata Model Shown in Figure 4-12 [y-axis: Acceleration (m/s^2), x-axis: Time (s)]

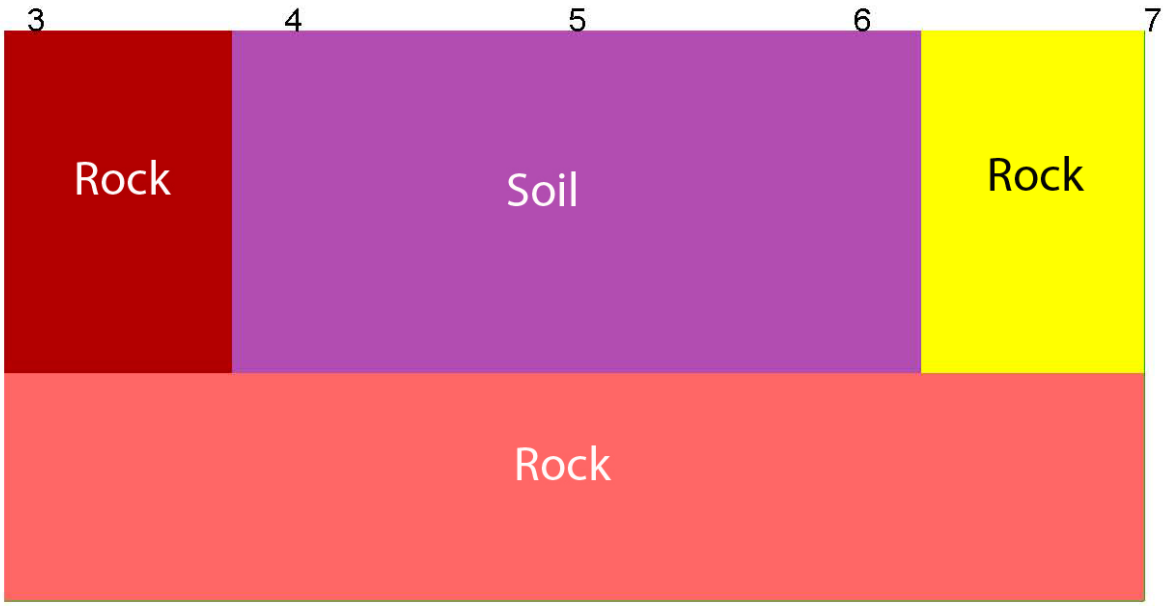

Figure 4-19. Basin Model Used With Monitoring Points (Note All Three Rock Blocks Have The Same Properties)

Table 4-8. Material Properties Used in Simulations						
Case	**Soil**			**Rock**		
	Density (kg/m^3)	**Bulk Modulus (GPa)**	**Shear Modulus (GPa)**	**Density (kg/m^3)**	**Bulk Modulus (GPa)**	**Shear Modulus (GPa)**
1	1,852	2.83	0.94	2,127	11.90	7.63
2	1,852	2.83	0.94	2,321	14.00	5.82
3	1,852	2.83	0.94	2,200	26.40	19.78

Table 4-9. Impedance Ratio Between Rock and Soil Used in Simulations	
Case	**Impedance Ratio (Z_{Rock}/Z_{Soil})**
1	2.79
2	3.05
3	5.00

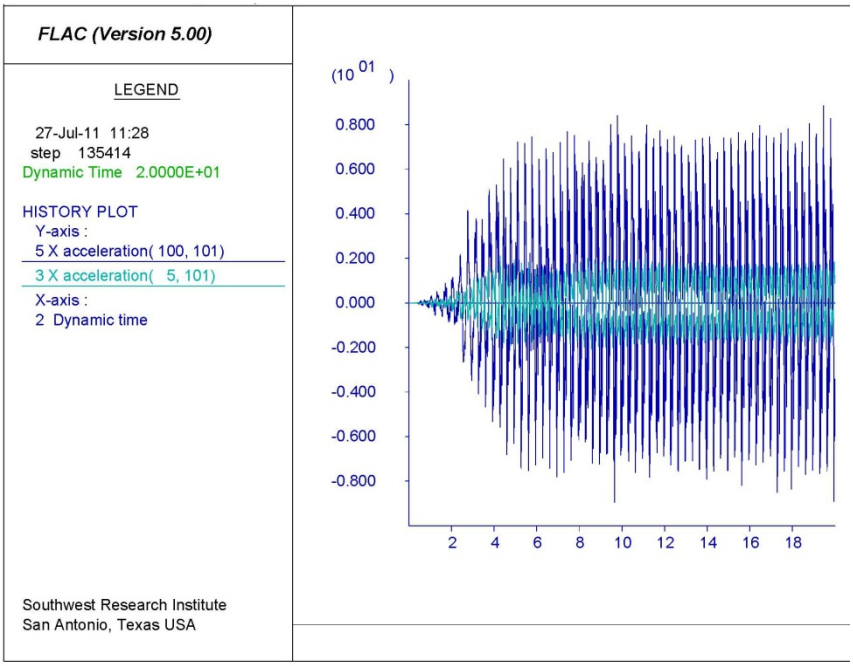

Figure 4-20. Comparison of Seismic Wave Amplification Between Rock and Soil at the Center of the Basin (Impedance Ratio 5.0) [y-axis: Acceleration (m/s^2), x-axis: Time (s)]

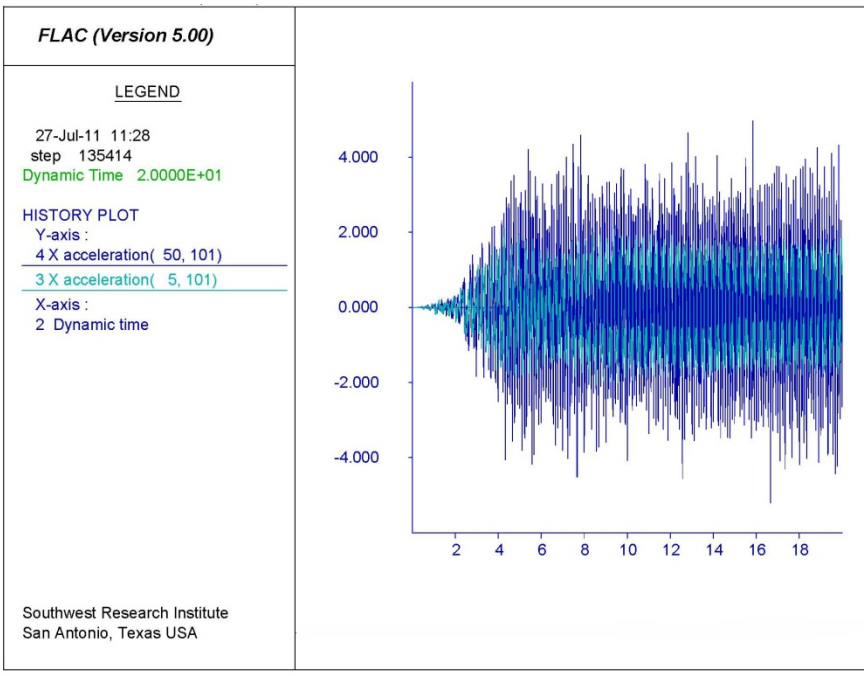

Figure 4-21. Comparison of Seismic Wave Amplification Between Rock and Soil at the Edge of the Basin (Impedance Ratio 5.0) [y-axis: Acceleration (m/s^2), x-axis: Time (s)]

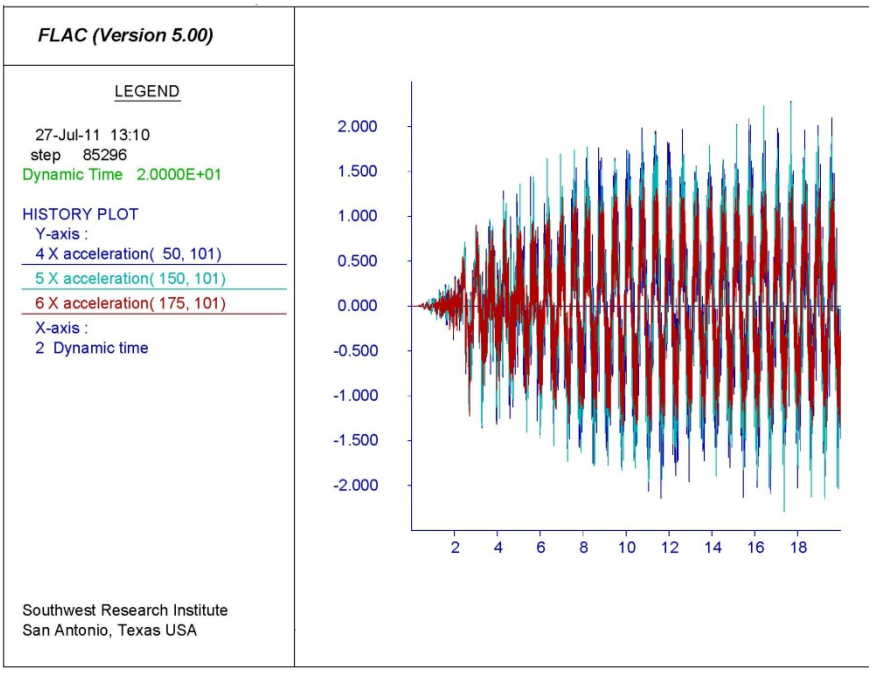

Figure 4-22. Comparison of Seismic Wave Amplification Across the Soil Basin (Seismic Impedance Ratio 2.79) [y-axis: Acceleration (m/s^2), x-axis: Time (s)]

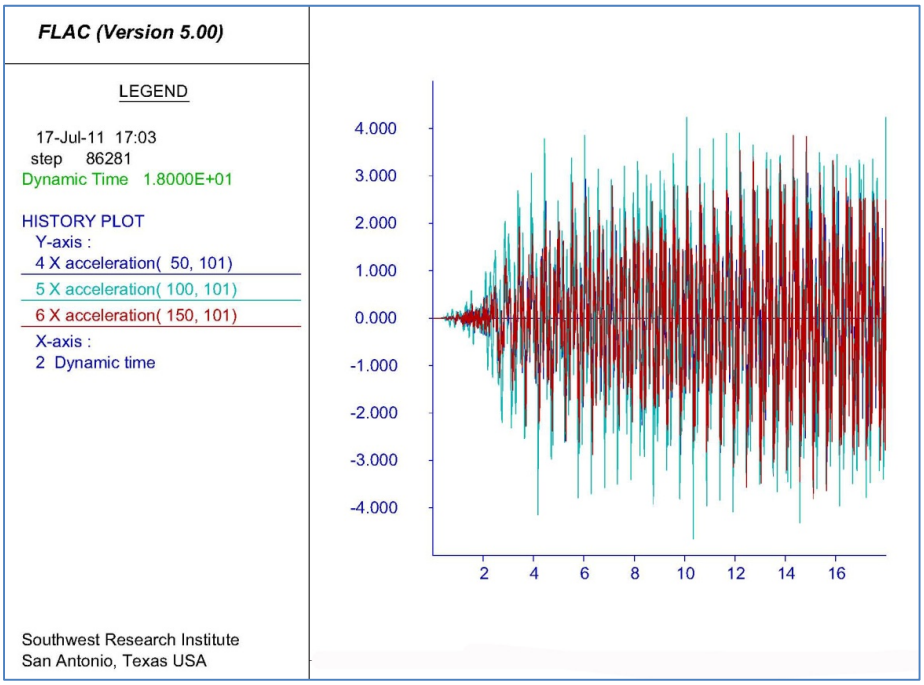

Figure 4-23. Comparison of Seismic Wave Amplification Across the Soil Basin (Seismic Impedance Ratio 3.05) [y-axis: Acceleration (m/s^2), x-axis: Time (s)]

Impedance contrast between the soil basin and the surrounding rock mass allows a small portion of the input seismic energy to dissipate in the rock mass. A large part of the input waves, once these propagate inside the soil basin, gets trapped by repeated reflections from the soil–rock interface. Only a small portion of the energy will be able to be transmitted back into the rock. This amplification in the soil basin will be more severe as the impedance contrast between the rock and soil increases. As the soil is significantly weak, it undergoes severe deterioration of the shear modulus. The soil mass may transform practically into an almost liquefied state with small rigidity to resist the seismic motion, especially with Case 3 having the impedance ratio 5.0. As a result, the soil mass vibrates significantly under the load from the trapped seismic waves. It is expected that the oscillation will continue for a significantly longer duration.

Figures 4-25 and 4-26 show the spectral acceleration plots across the soil basin with impedance ratios 3.05 and 5.0, respectively. These figures show that the middle of the basin vibrates more in resonance than the regions near the soil–rock interface.

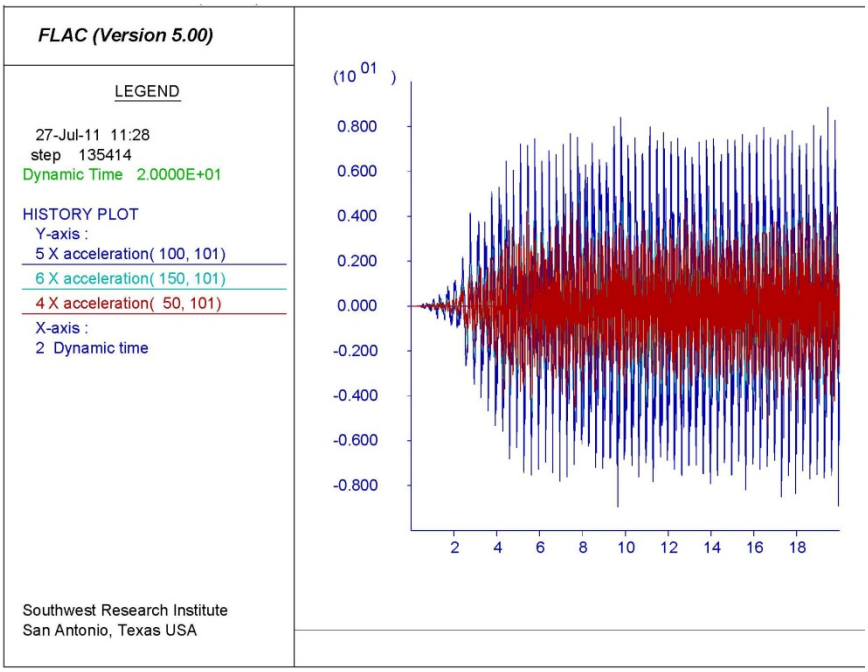

Figure 4-24. Comparison of Seismic Wave Amplification Across the Soil Basin (Seismic Impedance Ratio 5.0) [y-axis: Acceleration (m/s^2), x-axis: Time (s)]

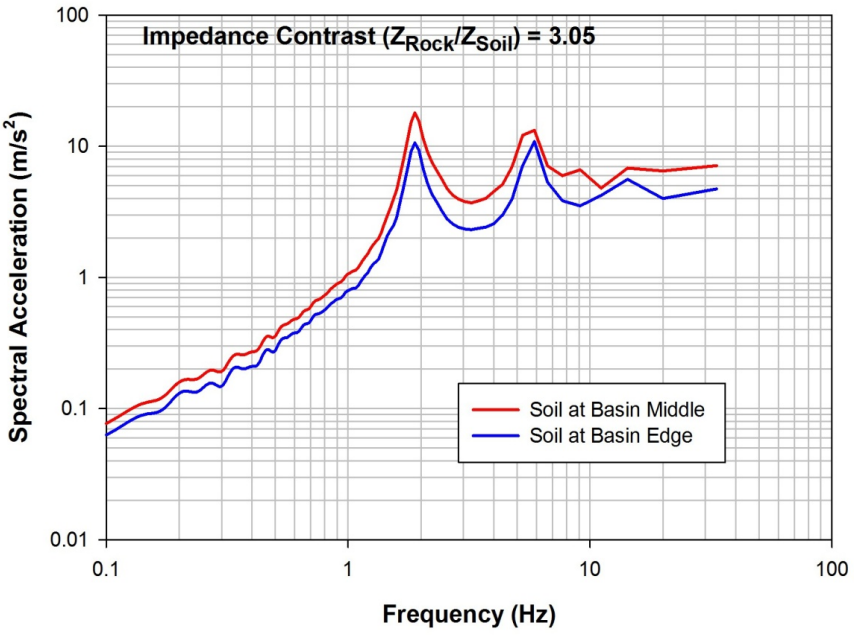

Figure 4-25. Comparison of Spectral Acceleration Across the Soil Basin (Seismic Impedance Ratio 3.05)

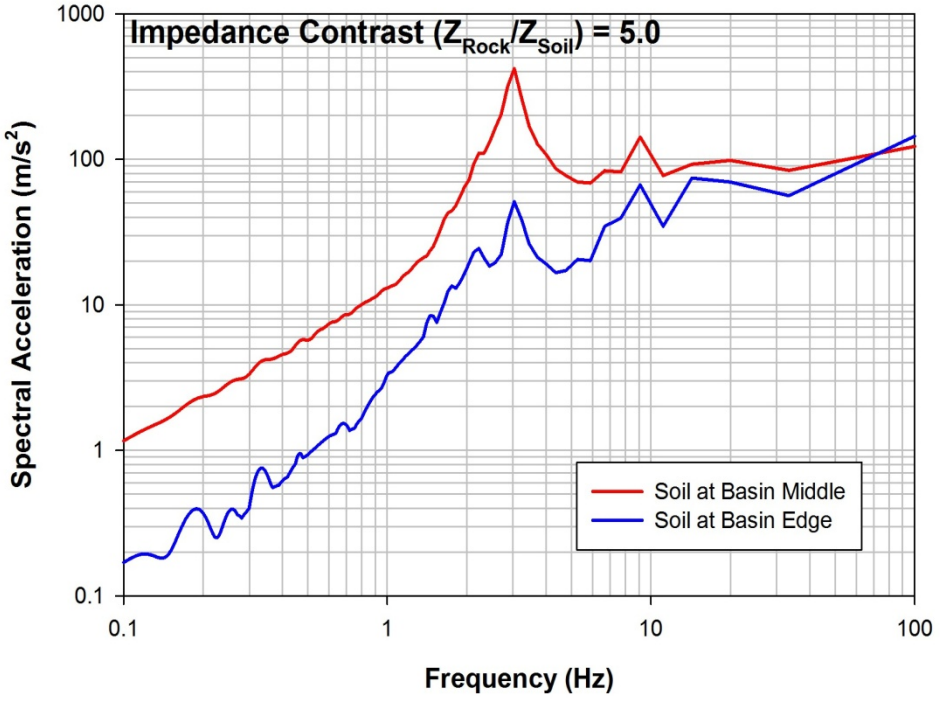

Figure 4-26. Comparison of Spectral Acceleration Across the Soil Basin (Seismic Impedance Ratio 5.0)

5 SUMMARY AND CONCLUSIONS

In this study, 2D analyses have been conducted to assess the ground motion to be expected at the top surface of a layered, faulted, and fractured deposit subjected to an earthquake. The rock mass in this model is overlain by a thick soil layer. The rock mass is composed of several different layers of rock with widely varying properties, including shear wave velocity. The analyses used the reference geology and materials properties data, particularly the measured values of degraded shear modulus with increasing shear strain, from the proposed geologic repository site at Yucca Mountain, Nevada (Bechtel SAIC Company, LLC, 2004). . The recorded motion from the Coalinga1 earthquake (Hsiung, et al., 2007) was applied at the bottom of the modeled region, generally at a depth of 200 to 260 m [656 to 853 ft] from the ground surface. Simulations were conducted using two widely used computer programs in soil and rock engineering UDEC (Itasca Consulting Group, 2011) and FLAC (Itasca Consulting Group, 2005). This report documents the results obtained from the analyses. The analyses results are preliminary and should not be used in a licensing proceeding until further investigation is conducted on the estimated ground response.

UDEC has the capability to model numerous intersecting fractures easily. Consequently, UDEC was used to assess the effects of a faulted and jointed rock mass on wave propagation. UDEC is a discontinuum code: a major portion of the rock mass deformation is realized by fracture deformation and slippage, which moves the intact rock blocks. Currently, the UDEC code does not have a constitutive model for the block material that can simulate the nonlinear shear modulus degradation as a function of shear strain, as shown in Figures 2-2 and 2-3 In this analysis, only linear elastic behavior of the intact rock blocks was used. Consequently, these analyses do not capture the rock shear strain effects on the seismic waves as they pass through a rock or soil layer.

Results of UDEC analysis show the following:

(1) Amplification of the input seismic waves increases with increase in soil thickness above the rock mass as the soil has a lower modulus of rigidity and, hence, slower shear wave velocity than the rock.

(2) Stiffness properties of the fractures (both joints and faults) in the rock mass also influence the seismic motion at the ground surface; lower stiffness properties make the overall material less stiff, and as a result, the material amplifies the seismic motion more. The amplification observed in this study was generally less than 1.6 times the original peak motion.

(3) Because UDEC can only simulate linear elastic deformation of the blocks, the estimated amplification of the seismic waves at the ground surface is low, compared to the wave amplification obtained from FLAC analysis.

To assess the effects of shear modulus reduction of the rock and soil layers as a function of induced shear strain on the surface ground motion, the computer code FLAC was used. Three built-in models of FLAC were used to represent the modulus degradation as the waves pass through. Note that FLAC is a continuum code, unlike UDEC. Consequently, it cannot simulate the presence of multiple intersecting fractures. Effects due to both horizontal and inclined strata

layers were assessed using the FLAC code. In addition, a soil basin model was analyzed to assess the effects of impedance mismatch between the soil and the surrounding rock medium. Results of FLAC analysis show the following:

(1) Response at the ground surface is affected by material layers with different thickness and material properties, similar to that in UDEC analysis. Response at the ground surface is also affected by the shear modulus reduction with shear strain as a result of the hysteretic damping of each layer at the site. An amplification of approximately 9.5 times was observed for the geometry of soil and rock layers including their material properties used in this analysis. This amplification factor is expected to be different for other material geometries with different properties because these are site-specific parameters.

(2) In the inclined strata model, the length of the path to be traversed by the vertically propagating wave through each material layer increases. This increased path length renders additional effects on the surface ground motion, which is expected to be proportional to the extra path length, other parameters remaining the same.

(3) In the basin model, amplification of the ground motion is largely controlled by the impedance contrast between the soil and the surrounding rock. As the impedance contrast increases (higher Z_{Rock}/Z_{Soil} ratio), the seismic wave amplitude inside the soil basin increases significantly. Moreover, the wave amplification varies spatially. The amplification is lower near the edges and increases toward the middle of the basin.

(4) A soil basin with high impedance contrast with the surrounding medium appears to trap seismic wave energy within the basin. If the seismic energy is sufficient (large shear strain) to reduce the modulus significantly, the response motion could have a large magnitude and significantly long duration.

(5) Strong ground motion may significantly affect the response at the ground surface. It seems that the shear modulus of rock and soil reduces significantly and the damping ratio increases, following the curves shown in Figures 2-2 and 2-3, when the first major pulse of the input ground motion arrives. Alluvium (soil) undergoes more shear modulus reduction than rock (Figures 2-2 and 2-3). Both materials thereafter respond to the incoming waves by developing oscillatory pulses with large amplitude; amplification approximately 9.5 times has been observed in this study. Bielak, et al. (1999) observed eight times amplification of the seismic motion over thick soil deposits in Armenia from the 1988 Armenia earthquake. Kramer (1996) indicated alluvial valleys can generate a very complex, even chaotic, motion.

(6) Estimated acceleration histories using the layered media and the basin model (Figures 4-14, 4-16, 4-17, 4-18, 4-20–4-24) indicate resonant behavior. Plots of spectral acceleration (Figures 4-25 and 4-26) also show concentration of energy at different frequencies, indicating resonant behavior. Moreover, the frequencies at which resonant behavior was observed vary with the material properties. The resonant frequencies are higher with larger seismic impedance ratio, as can be seen in Figures 4-25 and 4-26. Similar resonant response has been observed in measured and analyzed responses over thick soil deposits in other studies [e.g., Bielak, et al. (1999, Figure 6); Kramer (1996, Figure 8.15)]. Bielak, et al. (1999) observed vibration of soil at four resonant frequencies near the deepest part of the soil deposit. The stiffer region vibrated at only one resonant frequency.

This study did not conduct 1D simulations. As a result, quantitative differences between 1D and 2D analyses could not be assessed; however, the trend observed in the estimated ground motion in the 2D analyses is similar to that observed in other studies in which 1D and 2D simulations were directly compared (e.g., Bielak, et al., 1999). Bielak, et al. (1999) observed higher amplification across the valley with deep soil deposits. Similar observations can be made for the basin model in this analysis (Section 4.2.4).
Bielak, et al. (1999) noted that the spatial variation of site response cannot be reproduced using 1D analysis. In addition, Bielak, et al. (1999) observed resonant behavior in 2D simulations at slightly higher frequencies than that observed in 1D simulation. They attributed this behavior to lateral confinement provided by the valley. Additionally, they observed resonant behavior at frequencies not observed in 1D simulation.

6 REFERENCES

Arslan, H. and B. Siyahi. "A Comparative Study of Linear and Nonlinear Site Response Analysis." *Environmental Geology*. Vol. 50. pp. 1,193–1,200. 2006.

Bardet, J.P., I.M. Idriss, T.D. O'Rourke, N. Adachi, M. Hamada, and K. Ishihara. "North America Japan Workshop on the Geotechnical Aspects of the Kobe, Loma Prieta, and Northridge Earthquakes." Report to National Science Foundation, Air Force Office of Scientific Research, and Japanese Geotechnical Society. Kobe, Japan: National Science Foundation. 1997.

Bardet, J.P., M. Kapuskar, G.R. Martin, and J. Proubet. "Site Response of the Marina District of San Francisco During the Loma Prieta Earthquake." *The Loma Prieta, California, Earthquake of October 17, 1989; Marina District; Strong Ground Motion and Ground Failure*. T.D. O'Rourke and T.L. Holzer, eds. U.S. Geological Survey Professional Paper 1551-F. Denver, Colorado: U.S. Geological Survey. pp. 85–140. 1992.

Bechtel SAIC Company, LLC. "Development of Earthquake Ground Motion Input for Preclosure Seismic Design and Postclosure Performance Assessment of Geologic Repository at Yucca Mountain, Nevada." MDL–MGR–GS–000003. Rev. 01. Las Vegas, Nevada: Bechtel SAIC Company, LLC. 2004.

Bielak, J., J. Xu, and O. Ghattas. "Earthquake Ground Motion and Structural Response in Alluvial Valleys." *Journal of Geotechnical and Geoenvironmental Engineering*. Vol. 125. pp. 413–423. 1999.

Bielak, J., K. Loukakis, Y. Hisada, and C. Yoshimura. "Domain Reduction Method for Three-Dimensional Earthquake Modeling in Localized Regions, Part I: Theory." *Bulletin of the Seismological Society of America*. Vol. 93. pp. 817–824. 2003.

EPRI. "Guidelines for Determining Design Basis Ground Motion." Palo Alto, California: Electric Power Research Institute. Vol. 1, Appendix 7.A. 1993.

Frankel, A. "Three-Dimensional Simulations of Ground Motions in the San Bernardino Valley, California, for Hypothetical Earthquakes on the San Andreas Fault." *Bulletin of the Seismological Society of America*. Vol. 83. pp. 1,020–1,041. 1993.

Graves, R.W. "Modeling Three-Dimensional Site Response Effects in the Marina District Basin, San Francisco, California." *Bulletin of the Seismological Society of America*. Vol. 83, No. 4. pp. 1,042–1,063. 1993.

Hartzell, S., A. Leeds, A. Frankel, and J. Michael. "Site Response for Urban Los Angeles Using Aftershocks of the Northridge Earthquake." *Bulletin of the Seismological Society of America*. Vol. 86. pp. 168–192. 1996.

Hsiung, S.M., A. Ghosh, and A.H. Chowdhury. "Site Response and Soil–Structure Interaction Analyses—A Progress Report." San Antonio, Texas: Center for Nuclear Waste Regulatory Analyses. 2007.

Hsiung, S.M., D.D. Kana, M.P. Ahola, A.H. Chowdhury, and A. Ghosh. NUREG/CR–6178, "Laboratory Characterization of Rock Joints." San Antonio, Texas: Center for Nuclear Waste Regulatory Analyses. 1994.

Itasca Consulting Group, Inc. "UDEC Version 5.0 User's Guide." Minneapolis, Minnesota: Itasca Consulting Group, Inc. 2011.

Itasca Consulting Group, Inc. "FLAC Fast Lagrangian Analysis of Continua User's Guide (Version 5.0)." Minneapolis, Minnesota: Itasca Consulting Group, Inc. 2005.

Kramer, S.L. *Geotechnical Earthquake Engineering*. Upper Saddle River, New Jersey: Prentice Hall. 1996.

Schnabel, P.B., J. Lysmer, and H.B. Seed. "SHAKE: A Computer Program for Earthquake Response Analysis of Horizontally Layered Sites." EERC72–12. Berkeley, California: University of California. 1972.

Xu, J., J. Bielak, O. Ghattas, and J. Wang. "Three-Dimensional Nonlinear Seismic Ground Motion Modeling in Basins." *Physics of the Earth and Planetary Interiors*. Vol. 137. pp. 81–95. 2003.

Yoshimura, C., J. Bielak, Y. Hisada, and A. Fernandez. "Domain Reduction Method for Three-Dimensional Earthquake Modeling in Localized Regions, Part II: Verification and Applications." *Bulletin of the Seismological Society of America*. Vol. 93. pp. 825–840. 2003.

Zhang, B. and A.S. Papageorgiou. "Simulation of the Response of the Marina District Basin, San Francisco, California, to the 1989 Loma Prieta Earthquake." *Bulletin of the Seismological Society of America*. Vol. 86. pp. 1,382–1,400. 1996.

APPENDIX
HYSTERETIC DAMPING

APPENDIX—ESTIMATION OF CONSTANTS FOR HYSTERETIC DAMPING MODELS

The equivalent linear method (e.g., SHAKE analysis) assumes linearity in the solution process. Therefore, strain-dependent modulus and damping functions are taken in an average sense. To approximate the nonlinear effects of material softening and damping, as shown in Figures 2-1 and 2-2, FLAC can model hysteretic damping, which does not drastically reduce the timesteps. In the FLAC formulation, the mean strain rate tensor is calculated before any calls to the constitutive model. The constitutive model then uses the normalized tangent modulus as the multiplier for adjusting the apparent tangent shear modulus of the full zone being processed. In earthquake engineering, the modulus degradation curves are usually available as tables of values with cyclic strains spaced logarithmically. Because a derivative of this curve is necessary to represent the normalized tangent modulus, the coarse spacing of the tabular values may lead to unacceptable errors when derivatives are calculated numerically. Consequently, analytical models should be fitted to the tabular data before simulations using FLAC can be conducted. In this analysis, three models of FLAC (Itasca Consulting Group, Inc., 2005) have been used to represent the hysteretic damping of materials, as described next. The normalized shear modulus and material damping with respect to shear strain used in this analysis are given in Tables A–1 and A–2 for tuff (Tmbt1 through Tpcyln) and alluvium (Qal), respectively.

Data presented in Tables A–1 and A–2 are plotted in Figures A–1 and A–2, respectively.

Default Model

The modulus versus logarithm of cyclic strain curve is S shaped and can be represented by a cubic equation with zero slope at both ends (at both low and high strains). The secant modulus M_s is

$$M_S = s^2(3 - 2s)$$

where

$$s = \frac{L_2 - L}{L_2 - L_1}$$

and L is the logarithmic strain

$$L = \log_{10}(\gamma) \quad ,$$

where L_1 and L_2 are the strain values with zero slopes. Thus, putting $L_1 \tilde{=} 3$ and $L_2 = 1$ extends that the S curve from a low cyclic strain of 10^{-3} or 0.001 percent to a high cyclic strain of 10^{1} or 10 percent.

Sigmoidal Models Sig3 and Sig4

Sigmoidal curves can be used to represent modulus degradation curves. Two models with 3 (Sig3) and 4 (Sig4) parameters are

$$M_s = \frac{a}{1 + \exp\left[-\left(L - x_0\right)/b\right]}$$

and

$$M_s = y_0 + \frac{a}{1 + \exp\left[-\left(L - x_0/b\right)\right]}$$

These three models were fitted to the data presented in Tables A–1 and A–2. The fitted parameters are given next:

Default Model

Tuff	Alluvium		
L_1	3.425	L_1	3.425
L_2	3.23	L_2	0.823

Sig3 Model Parameters

Tuff	Alluvium		
a	0.997	a	1.012
b	−0.3034	b	−0.4753
x_0	−0.2334	x_0	−1.1418

Sig4 Model Parameters

Tuff	Alluvium		
a	341.99	a	1.0217
b	−0.5125	b	−0.4837
x_0	3.2271	x_0	−1.1322
y_0	−340.9961	y_0	-8.07×10^{-3}

Figures A–3 and A–4 show the fit of these parameters to the data obtained at the Yucca Mountain site for “Upper Mean Tuff” and “Upper Mean Alluvium” (Bechtel SAIC, Company, LLC, 2004).

REFERENCES

Bechtel SAIC Company, LLC. “Development of Earthquake Ground Motion Input for Preclosure Seismic Design and Postclosure Performance Assessment of Geologic Repository at Yucca Mountain, Nevada.” MDL–MGR–GS–000003. Rev. 01. Las Vegas, Nevada: Bechtel SAIC Company, LLC. 2004.

Itasca Consulting Group, Inc. "FLAC Fast Lagrangian Analysis of Continua User's Guide (Version 5.0)." Minneapolis, Minnesota: Itasca Consulting Group, Inc. 2005.

Table A–1. Measured Damping Data for Tuff (Tmbt1 Through Tpcyln)*		
Average Shear Strain (Percent)	**Normalized Shear Modulus**	**Material Damping Ratio**
1.0000×10^{-4}	1.0000	0.5000
3.0000×10^{-4}	1.0000	0.5000
1.0000×10^{-3}	1.0000	0.5000
3.2000×10^{-3}	1.0000	0.5000
0.0100	0.9900	0.5000
0.0316	0.9700	0.5000
0.1000	0.8700	2.5400
0.3162	0.7000	5.6300
1.0000	0.4600	10.5900
1.3162	0.0800	15.0000

*Bechtel SAIC Company, LLC. "Development of Earthquake Ground Motion Input for Preclosure Seismic Design and Postclosure Performance Assessment of Geologic Repository at Yucca Mountain, Nevada." MDL–MGR–GS–000003. Rev. 01. Las Vegas, Nevada: Bechtel SAIC Company, LLC. 2004.

Table A–2. Measured Damping Data for Alluvium (Qal)*		
Average Shear Strain (Percent)	**Normalized Shear Modulus**	**Material Damping Ratio**
1.0000×10^{-4}	1.0000	0.7000
3.0000×10^{-4}	1.0000	0.8000
1.0000×10^{-3}	1.0000	0.8000
3.2000×10^{-3}	0.9700	1.1200
0.0100	0.8700	1.8000
0.0316	0.6800	3.5300
0.1000	0.4300	7.1000
0.3162	0.2200	12.7800
1.0000	0.0900	15.0000
1.3162	0.0500	15.0000

*Bechtel SAIC Company, LLC. "Development of Earthquake Ground Motion Input for Preclosure Seismic Design and Postclosure Performance Assessment of Geologic Repository at Yucca Mountain, Nevada." MDL–MGR–GS–000003. Rev. 01. Las Vegas, Nevada: Bechtel SAIC Company, LLC. 2004.

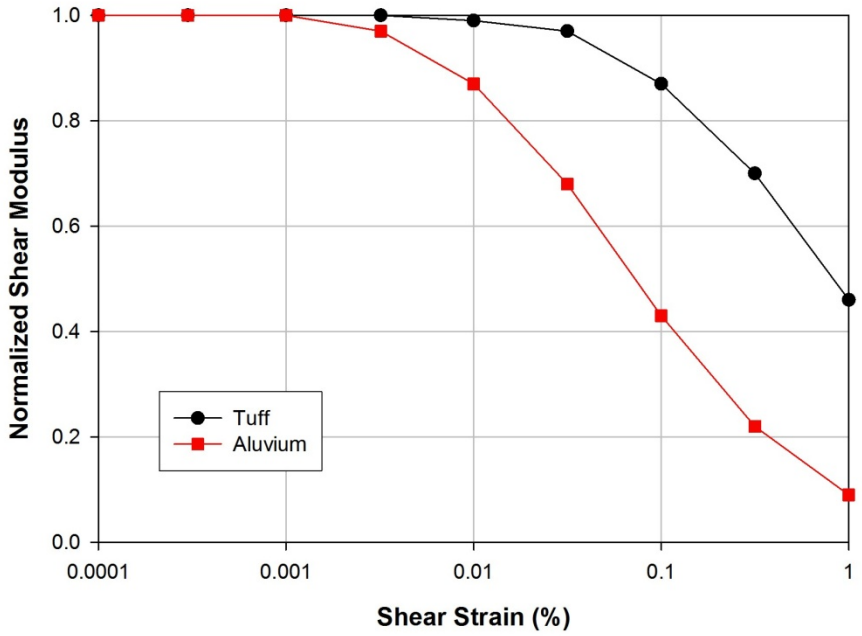

Figure A–1. Variation of Normalized Shear Modulus With Shear Strain Using Data for Upper Mean Tuff and Upper Mean Alluvium From Bechtel SAIC Company, LLC (2004)

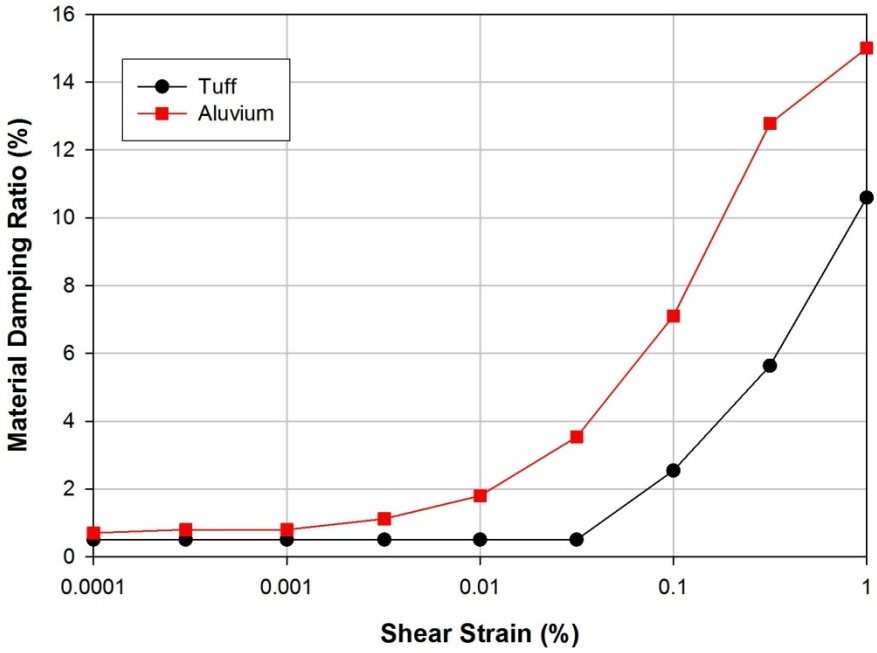

Figure A–2. Variation of Material Damping Ratio With Shear Strain Using Data for Upper Mean Tuff and Upper Mean Alluvium From Bechtel SAIC Company, LLC (2004)

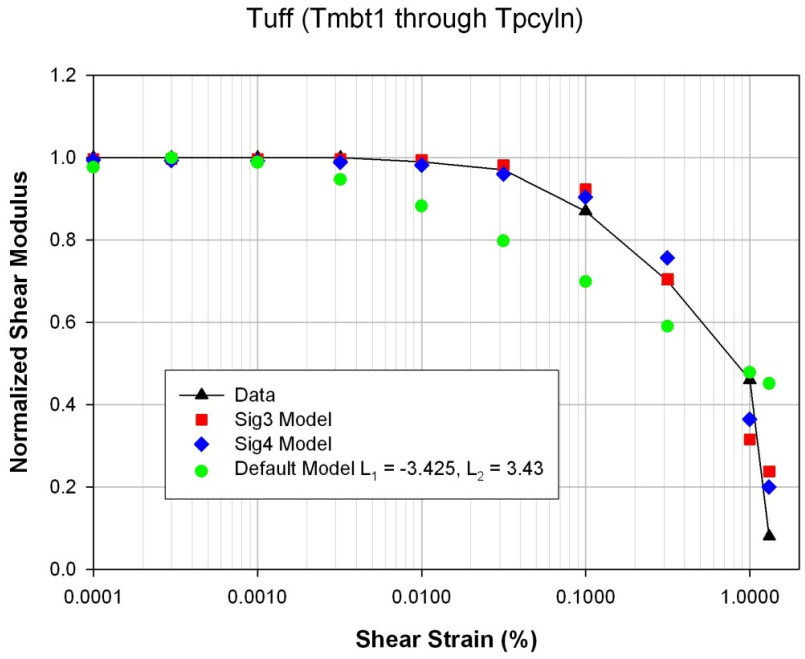

Figure A–3. Fit of Three Hysteretic Damping Models to Damping Data of Tuff From Bechtel SAIC Company, LLC (2004)

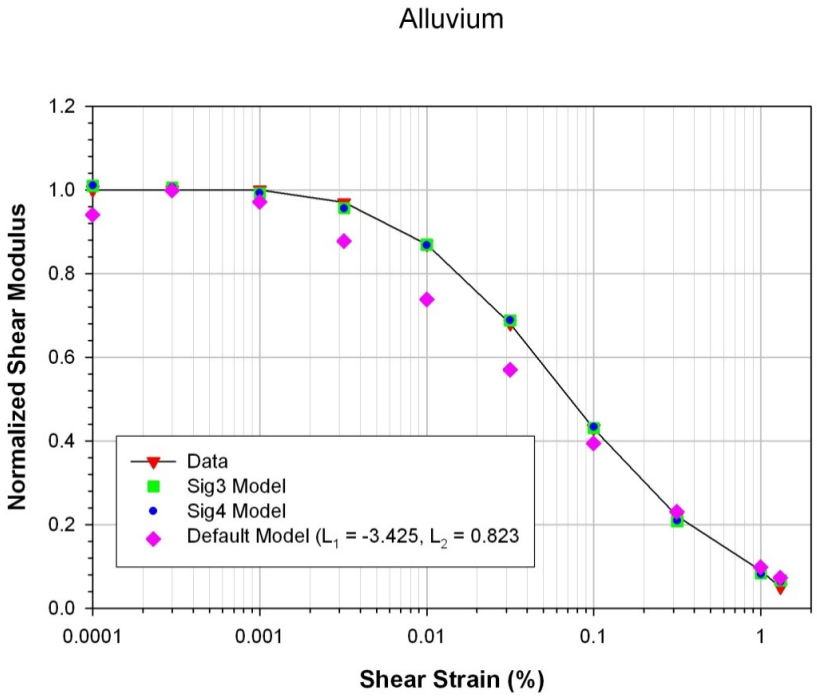

Figure A–4. Fit of Three Hysteretic Damping Models to Data of Alluvium From Bechtel SAIC Company, LLC (2004)